Periodica Polytechnica Civil Engineering, 70(2), pp. 612–631, 2026

Mechanical Behavior of a Guabirotuba Formation Soil Stabilized with Lime, Silica Fume, and Polypropylene Fibers

Edwin González-Rodríguez[1], Wagner Teixeira[1], Vitor E. P. Ribeiro[1], Arturo B. Tapia[1], Ronaldo Luis dos Santos Izzo[1*]

[1] Department of Civil Construction, Federal University of Technology - Paraná, Campus Curitiba, 5000 Dep. Heitor Alencar Furtado St., 81280-340 Ecoville, Paraná, Brazil
[*] Corresponding author, e-mail: izzo@utfpr.edu.br

Received: 02 February 2026, Accepted: 20 May 2026, Published online: 11 June 2026

Abstract

Problematic expansive soils from the Guabirotuba Formation present engineering challenges, some of them are low shear strength and high compressibility. This research addresses these problems by evaluating the mechanical behavior of this soil when stabilized with lime-activated silica fume (SF) and reinforced with polypropylene fibers (PPF). The experimental program evaluated mixtures containing 6–12% SF, 9% lime, and 0.5% PPF through unconfined compressive strength (UCS), splitting tensile strength (STS), and consolidated undrained (CU) triaxial tests, alongside scanning electron microscopy (SEM). The main findings reveal that lime is essential to activate the pozzolanic reaction of SF. The lime-SF blends form a Calcium Silicate Hydrate (C–S–H) matrix, significantly increasing UCS and STS. While the inclusion of PPF slightly reduced peak STS and had a negligible effect on peak UCS, its primary contribution was transforming the failure mode from brittle to ductile by bridging micro-cracks and preventing abrupt failure. Furthermore, triaxial testing demonstrated that fiber reinforcement consistently increases effective cohesion (c') but decreases the effective friction angle (ϕ'). SEM analysis corroborated these macroscopic findings, illustrating a densified matrix and strong fiber-matrix adhesion. This study demonstrates that the synergistic use of lime, SF, and PPF enhances the mechanical stability and ductility of Guabirotuba soil, which is relevant in geotechnical engineering applications such as pavement layers, embankments, and earth structures where enhanced post-peak behavior and structural integrity are desirable.

Keywords

soil stabilization, triaxial test, silica fume, lime, polypropylene fibers

1 Introduction

Expansive and dispersive clays have long been the focus due to their failure under precipitation or other moisture conditions. These soils are also known for their inferior engineering behaviors, such as their extremely high compressibility and low shear strength. To improve their mechanical properties, clays are recognized as having satisfactory results when modified with calcium-based cement agents, such as lime, cement, and fly ash [1–5].

The soil from the Guabirotuba Formation, predominantly found in the Curitiba region of southern Brazil, poses challenges to engineering projects [6]. These soils are mainly classified as high-plasticity clays or high-plasticity silts, characterized by a high natural moisture content, a high plasticity index, and expansiveness [6]. Another problematic feature is its fractured structure and a texture locally known as "sabão de caboclo" (in English: slippery clay), which becomes slippery when wet, thereby compromising the stability of slopes and excavations [7].

To overcome these limitations, this research proposes to explore the coupling effect of silica fume lime-activated and polypropylene fibers for stabilization of the pink Guabirotuba soil. The aim is to evaluate the mechanical behavior of a Guabirotuba soil stabilized with lime-activated silica fume (SF) and reinforced with polypropylene fibers (PPF). This combination is not only soil improvement but also aligns with the criteria of sustainability and the reuse of industrial by-products like silica fume [8, 9]. The use of recycled materials enhances sustainability, aligning with the Sustainable Development Goals (SDGs) by promoting a circular economy [10, 11].

Lime, widely used for stabilizing clayey soils, modifies their properties through cation exchange, flocculation, and

Cite this article as: González-Rodríguez, E., Teixeira, W., Ribeiro, V. E. P., Tapia, A. B., Izzo, R. L. S. "Mechanical Behavior of a Guabirotuba Formation Soil Stabilized with Lime, Silica Fume, and Polypropylene Fibers", Periodica Polytechnica Civil Engineering, 70(2), pp. 612–631, 2026.
https://doi.org/10.3311/PPci.43469

pozzolanic reactions with the silica and alumina present in the soil. When silica fume, a highly reactive by-product of industry, is mixed with lime, it speeds up the formation of calcium silicate hydrate (C–S–H) gels. This effect makes the soil stronger, less plastic, and more durable [12–14]. Concurrently, polypropylene fibers provide complementary mechanical benefits, such as increased tensile strength, improved ductility, and a reduction in drying shrinkage [15–17].

Soil reinforcement using fibers randomly distributed in the soil has been done with both natural and synthetic material. The synthetic fibers are usually polypropylene, polyester, polyethylene, glass, nylon, steel, and polyvinyl alcohol [18]. It is known that the strength of fiber-reinforced soil increases with an increase in aspect ratio, fiber content, fiber modulus, and soil-fiber surface friction. With respect to natural fibers, noteworthy materials include bamboo, jute, coir, palm, sugarcane bagasse, rice husks, sisal, and many others [17].

Mir Moayed et al. [19] investigated a kaolinite clay soil stabilized with nano-silica and reinforced with hemp fibers under freeze-thaw cycles. Mir Moayed et al. [19] conducted unconfined compression strength tests and determined that 1% of nano-silica yielded the maximum improvement. The most successful ratio for increasing soil strength in the 1% nano-silica was the inclusion of 0.4% hemp fibers. The addition of hemp fibers and nano-silica enhanced cohesion and friction among soil particles.

Recently, Zaid et al. [20] demonstrated that glass fiber reinforcement significantly improves the fracture resistance and crack propagation behavior of compacted clay liners. They observed that a fiber content of 0.01% yielded the optimal performance across different soil moisture conditions. Dou et al. [16] investigated a local silty clay soil reinforced with polypropylene fibers and compared it with expanded polystyrene (EPS) granular content. Unconfined compressive strength tests indicated a reduction in strength with increasing EPS content; yet, the addition of polypropylene fibers successfully mitigated this decline, resulting in a maximum compressive strength of 1.93 MPa. Dou et al. [16] also performed freeze-thaw cycle tests (−18 °C to 20 °C) and validated the material's superior frost resistance, exhibiting markedly less strength loss.

Although previous studies have demonstrated the benefits of calcium-based stabilizers, reactive silica additives, and discrete fiber reinforcement for problematic soils, the available literature remains limited regarding their combined action in expansive residual soils, particularly in the Guabirotuba Formation, and their influences on the effective shear strength parameters.

To address this gap, the primary objective of this study is to evaluate the synergistic effects of lime-activated silica fume and polypropylene fibers on the mechanical behavior and microstructural evolution of the expansive soil from the Guabirotuba Formation. To achieve this, the specific objectives are: determine the optimal silica fume dosage (6%, 9%, or 12%) activated with a fixed 9% lime content to maximize unconfined compressive strength (UCS) and splitting tensile strength (STS); assess the impact of 0.5% polypropylene fiber inclusion on the ductility and failure mode of the stabilized matrix; evaluate the evolution of the effective shear strength parameters (c' and ϕ') through consolidated undrained (CU) triaxial testing; and elucidate the underlying chemical and mechanical stabilization mechanisms via scanning electron microscopy (SEM) and energy-dispersive X-ray spectroscopy (EDS) analyses.

2 Materials

2.1 Soil

For this study, a sample of pink-colored natural soil belonging to the Guabirotuba Formation was collected. The sample was collected manually from the municipality of Fazenda Rio Grande, Paraná (PR), Brazil, at the coordinates 25°41'44.5"S and 49°17'22.8"W.

The geotechnical properties of the natural Guabirotuba soil are summarized in Table 1. According to the Unified

Table 1 Soil parameters

Parameters	Value
Specific Gravity of Solids (G_s)	2.591
CBR swell – mod. effort (%)	7.07
CBR soaked – mod. effort (%)	0.90
Gravel (> 2 mm) (%)	3.39
Coarse Sand (2–0.6 mm) (%)	13.68
Medium Sand (0.6–0.2 mm) (%)	6.70
Fine Sand (0.2–0.06 mm) (%)	15.99
Silt (0.06–0.002 mm) (%)	57.42
Clay (< 0.002 mm) (%)	2.81
D_{60} (mm)	0.0594
D_{30} (mm)	0.0173
D_{10} (mm)	0.0049
Coefficient of Uniformity (C_u)	12.060
Coefficient of Curvature (C_c)	1.022
Liquid Limit (LL) (%)	47.18
Plastic Limit (PL) (%)	32.67
Plasticity Index (PI) (%)	14.51

Soil Classification System (USCS), the material is classified as a low-plasticity silt (ML). Despite the low clay content, the soil exhibits plastic behavior, which can be attributed to the influence of clay minerals. Recent comparative studies have demonstrated that this optical method systematically underestimates the true fraction of platy clay minerals when compared to traditional sedimentation methods [21]. Consequently, while the particle size yields an ML classification, the soil geomechanical, plastic and expansive behaviors are fundamentally governed by its clay mineralogy.

The chemical composition is mainly SiO_2 and Al_2O_3 (Table 2), which are common in sedimentary soils.

Scanning electron microscopy (Fig. 1) reveals a loosely packed fabric defined here as the arrangement of particles, particle groups, and pore spaces in the soil mass with an irregular surface, where particles are in contact rather than bonded. On the left side of Fig. 1 (a), fine and platy aggregates are visible, while a possible larger angular quartz grain is located on the right, along with general void spaces.

The EDS analysis (Table 3) confirms the mineralogical heterogeneity observed in Fig. 1. The elemental composition is predominantly composed of oxygen (O), aluminum (Al), and silicon (Si), identifying the main material as an aluminosilicate matrix. Significant concentrations of carbon (C) were detected at four of the five points analyzed,

Table 2 Chemical composition of silica fume, lime and soil (wt.%) determined by X-ray Fluorescence (XRF)

Composition	Soil	Silica fume	Lime
SiO_2	57.32	88.24	1.26
CaO	0.856	7.511	73.02
Al_2O_3	32.481	3.09	–
SO_3	5.422	0.347	7.562
MgO	–	–	18.56
K_2O	3.954	0.62	0.112
Fe_2O_3	0.224	0.02	0.04
TiO_2	0.306	0.18	–
P_2O_5	–	–	0.354

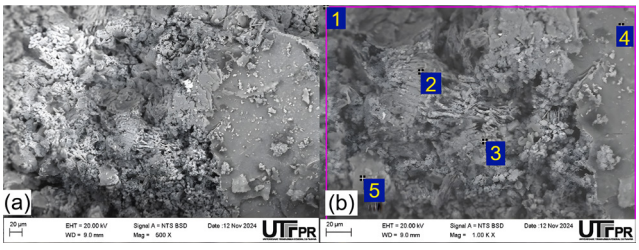

Fig. 1 Micrographs of natural soil: (a) at 500 X magnification; (b) at 1.0 kX magnification

Table 3 Energy Dispersive X-ray Spectroscopy (EDS) analysis of the soil

Pos.	C	O	Al	Ti	Fe
1	–	64.53	12.48	13.14	3.93
2	9.73	58.81	14.68	15.67	1.11
3	8.77	64.74	12.11	12.99	0.96
4	9.39	53.6	15.47	16.83	4.46
5	9.1	62.07	12.01	12.6	4.03

suggesting the presence of organic matter distributed in the mineral matrix. Iron (Fe) is present, probably in the form of oxides, which would explain the pinkish color of the soil.

2.2 Silica fume

The silica fume (SF) was obtained in the local market under the trade name of "Microsilica". This material is a fine grey powder, composed essentially of silicon dioxide (SiO_2). The particle size distribution of silica fume, lime, and soil (Fig. 2) was analyzed by BETTERSIZE/S3 PLUS equipment.

2.3 Lime

The lime is a CH-III dolomitic hydrated lime, commercially available under the brand name "Hidra". Chemically, it mainly consists of calcium hydroxide [$Ca(OH)_2$] and magnesium hydroxide [$Mg(OH)_2$] (Table 2).

The X-ray diffraction (XRD) patterns, which show the mineralogical compositions of the soil, lime, and silica fume, are presented in Fig. 3. In the soil, the analysis primarily identified the presence of quartz and kaolinite, with a low content of amorphous material or other phases. Kaolinite is a common expansive mineral in red or pink soils derived from igneous or metamorphic rocks. These minerals are frequently found in the fine fractions of tropical and subtropical soils in southern Brazil and are characteristic of expansive soils [22].

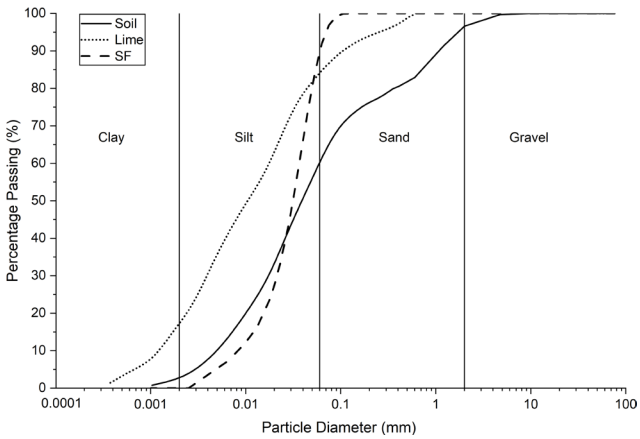

Fig. 2 Grain size distribution of soil, silica fume and lime

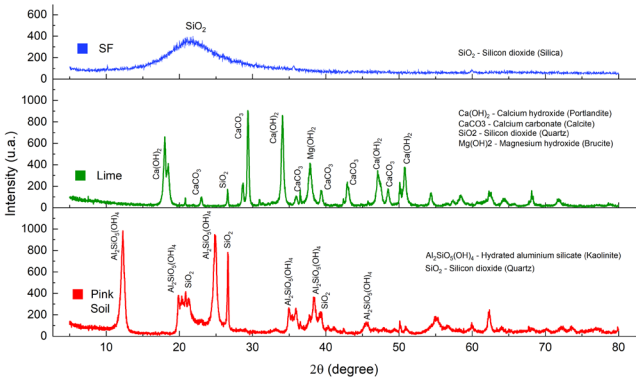

Fig. 3 X-ray Diffraction (XRD) analysis of silica fume, lime and soil

2.4 Polypropylene fibers

In this study, polypropylene fibers (PPF) with dimensions of 12 mm in length and 18 µm in diameter, a specific mass of 0.91 g/cm^3, and a melting and ignition temperatures of 160 and 365 °C, respectively, were employed.

3 Method

Table 4 shows the different blends and contents carried out for this study. The parameter selection was based on optimizing the stability of the Guabirotuba soil. A range of 6% to 12% silica fume (SF) was chosen because, although 6% is a documented optimum for some clays [23], it may require higher doses to achieve maximum strength [24]. A fixed content of 9% hydrated lime was selected for all stabilized mixtures. The Initial Consumption of Lime (ICL) reached a pH of 12.4 at 2% of lime, above this content, the pH stabilizes at 12.5 with 7% of lime. The 9% hydrated lime dosage was determined quantitatively based on ICL and regional stabilization criteria for the Guabirotuba Formation [25, 26], which also typically exhibits an ICL between 3% and 5%. The 9% dosage ensures that, after satisfying the soil's immediate calcium demand for cation exchange and flocculation, a residual buffer of approximately 4% to 6% of lime remains.

This excess is necessary to provide the high-pH environment and the free calcium ions required to activate the pozzolanic reaction of the high-surface-area silica fume, added at proportions up to 12. For the polypropylene fibers (PPF), a 0.5% content and 12 mm length were chosen, a combination that enhances ductility and crack control without negatively affecting workability [27]. Lastly, modified compaction energy was used to evaluate the maximum performance of the mixtures in high-demand applications [28].

The samples were cured in insulated expanded polystyrene (EPS) chambers with water reservoirs and sealed with EPS lids. This configuration created a stable, high-humidity environment (with relative humidity close to 100%), which kept moisture and allowed pozzolanic reactions.

3.1 Proctor test

A compaction test was conducted in all mixtures using the modified effort method in accordance with ASTM D1557-12(2021) standard [29] to determine the maximum dry density (MDD) and the moisture content (OMC).

The compaction tests (Table 5) indicate that the addition of silica fume (SF), lime, and polypropylene fibers (PPF) modifies the soil's properties. Compared to the soil, which has an optimum moisture content (OMC) of 15.00% and a maximum dry density (MDD) of 1.79 g/cm^3, all stabilized mixtures showed a reduction in maximum dry unit weight and an increase in optimum moisture.

The effect of the silica fume is progressive, as its content increases from 6% to 12%, the optimum moisture content rises from 17.80% to 20.05%, while the maximum dry unit weight decreases from 1.73 g/cm^3 to 1.66 g/cm^3. This behavior is attributed to the high specific surface area of silica fume, which demands a higher amount of water to properly lubricate the particles during compaction.

The incorporation of lime (mixtures S-SF6-L9 to S-SF12-L9) accentuates this trend. The maximum dry unit

Table 4 Blend content and curing periods

Sample	SF (%)	Lime (%)	PPF (%)	Curing (days)
Soil	0	0	0	0
S-SF6	6	0	0	7–14–28
S-SF9	9	0	0	7–14–28
S-SF12	12	0	0	7–14–28
S-SF6-L9	6	9	0	7–14–28
S-SF9-L9	9	9	0	7–14–28
S-SF12-L9	12	9	0	7–14–28
S-SF6-L9-PPF05	6	9	0.5	7–14–28
S-SF9-L9-PPF05	9	9	0.5	7–14–28
S-SF12-L9-PPF05	12	9	0.5	7–14–28

Table 5 Dry unit weight and optimum moisture content values

Sample	OMC (%)	MDD (g/cm^3)
Soil	15.00	1.79
S-SF6	17.80	1.73
S-SF9	19.02	1.69
S-SF12	20.05	1.66
S-SF6-L9	18.07	1.72
S-SF9-L9	18.87	1.69
S-SF12-L9	20.50	1.66
S-SF6-L9-PPF05	17.50	1.65
S-SF9-L9-PPF05	18.25	1.61
S-SF12-L9-PPF05	18.98	1.58

weight decreases because the lime induces flocculation of the soil particles, creating a more open structure that is consequently harder to densify.

Finally, the addition of polypropylene fibers (mixtures S-SF6-L9-PPF05 to S-SF12-L9-PPF05) causes the most significant reduction in the maximum dry unit weight. This is because the fibers act as a reinforcement that interferes with the rearrangement and packing of the soil particles during the compaction process. Additionally, the inherent low density of the fibers contributes to lowering the overall unit weight of the mixture.

In summary, the behavior is due to two main mechanisms: the replacement of soil particles with materials of a lower unit weight, such as silica fume and polypropylene fibers, and an alteration in the soil structure, where lime induces flocculation and the polypropylene fibers create a three-dimensional mesh that resists compaction.

3.2 Sample preparation and curing

For the unconfined compressive strength, splitting tensile strength, and consolidated undrained (CU) triaxial tests, cylindrical specimens with nominal dimensions of 50 mm in diameter and 100 mm in height were molded. For each mixture type and curing time, four specimens were molded, a number determined by a statistical analysis to ensure a 95% confidence level.

For the molding procedure, first, the required amounts of dry materials (soil, silica fume, and lime) were weighed on a balance with a precision of 0.01 g. No formal pre-compaction mellowing period was applied between mixing and compaction. To ensure the uniform dispersion of the polypropylene fibers and avoid segregation or the formation of clumps, a multi-layer manual mixing protocol was adopted. Initially, the solid materials (natural soil, silica fume, and lime) were completely homogenized in a dry state; subsequently, the fibers were added gradually in small increments, mixing simultaneously and continuously by hand to ensure fiber separation. Finally, the necessary amount of water was added, gradually, to reach the optimum moisture content of the different mixtures. This process was followed until a homogeneous composite.

All the specimens were molded under the optimum moisture content and maximum dry density conditions obtained from the modified energy compaction test. An amount of each mixture was weighed, placed in the mold in three layers of equal mass, and each layer was statically compacted using a manual hydraulic press. Finally, the specimens were demolded, wrapped in plastic film, identified, and stored in polystyrene boxes at an average ambient temperature of (23 ± 3) °C until reaching the corresponding curing times of 7, 14 and 28 days.

To ensure the quality of the process, the moisture content of each specimen was verified after rupture by drying the material in an oven at 105 ± 5 °C to a constant weight. This verification confirmed that the sealed curing process was effective, as the moisture content at the time of testing remained within a ±1% tolerance of the target Optimum Moisture Content (OMC) established during molding for each respective mixture. If the restrictions were not satisfied, the specimen was discarded.

3.3 Statistical analysis

The results underwent statistical treatment to determine the uncertainty associated with the strength values. This analysis considered both random errors, inherent to the variability of the experimental process, and systematic errors, associated with the precision of the equipment used. For each experimental condition, four specimens were tested ($N = 4$). In these tests, the mean strength and the sample standard deviation were calculated as initial steps for the analysis.

The random uncertainty, represented by the standard error of the mean (σ_m), was calculated by dividing the standard deviation (σ_p) by the square root of the number of samples (N). To determine the confidence interval, a 95% confidence level was considered, applying the critical value from the Student's t-distribution (t), which for three degrees of freedom is equal to 3.182. Thus, the final error for the confidence interval was determined by the product of Student's t-distribution (t) and the standard error of the mean (σ_m). This statistical estimation was conducted in accordance with the ISO 2602:1980 standard [30]. Consequently, the significance of the difference between the results was assessed by evaluating these confidence intervals, the mechanical performance of different mixtures is considered statistically different only when their 95% confidence intervals do not overlap, providing a clear criterion to distinguish actual material enhancements from experimental scatter.

3.4 Triaxial test

To determine the shear strength parameters, consolidated undrained (CU) triaxial compression tests were performed. The equipment is a Geocomp LoadTrac-II, a triaxial chamber, pressure and volume controllers, a strain-controlled loading press, and a computational data acquisition system, the setup of which can be seen in Fig. 4. The test procedure was divided into the following stages: specimen assembly, saturation, consolidation, and shearing.

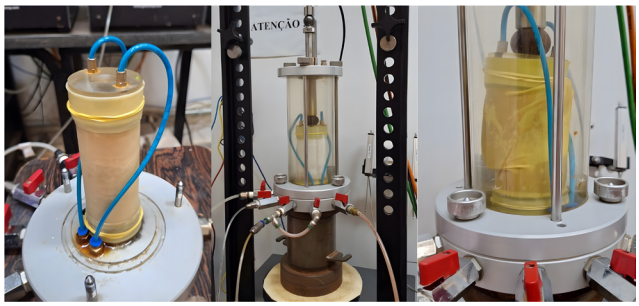

Fig. 4 Triaxial test (CU) process

For the Consolidated Undrained (CU) tests, individual specimens were evaluated at effective confining pressures of 50, 100, 200, and 400 kPa to construct the failure envelopes. Unlike the UCS and STS tests, replicates for each confining pressure were not performed due to the extended duration required for the saturation and consolidation phases. The effective shear strength parameters (c' and ϕ') were determined through linear regression analysis of the Mohr–Coulomb envelopes. The uncertainty of this fit was assessed using the coefficient of determination (R^2). The linear regressions yielded R^2 values consistently exceeding 0.95, indicating an adequate fit and low sensitivity of the derived parameters to experimental scatter.

In the assembly stage, the specimen was positioned on the pedestal of the triaxial chamber with a porous stone and filter paper at its base and top. It was then encased in a rubber membrane to make it impermeable, the chamber was subsequently sealed and filled with water. For saturation, an upward flow of water was applied through the specimen to remove air from its voids. The process was monitored by applying back pressure until Skempton's B-parameter reached a minimum value of 0.95, indicating that the sample was saturated.

In the consolidation stage, each specimen was subjected to a specific confining pressure. For each mixture, four specimens were tested, each consolidated under a confining stress of 50, 100, 200, or 400 kPa. Finally, in the shearing phase, the drainage valve was closed to ensure undrained conditions, and an axial load (σ_1) was applied at a constant strain rate of 1 mm/min until the specimen failed. This specific shearing rate was selected to align with testing standards for stabilized pavement materials [31]. Due to the cementitious matrix, the stabilized specimens exhibit semi-rigid behavior and higher initial permeability than natural pure clays. The maintenance of undrained conditions and adequate pore pressure equalization within the specimen were verified through the continuous and stable measurement of the excess pore water pressure at the sample throughout the shearing phase, which allowed for the calculation of the effective principal stresses.

3.5 Microstructural characterization (SEM/EDS)

Scanning Electron Microscopy (SEM) and Energy-Dispersive X-ray Spectroscopy (EDS) were used to qualitatively investigate the microstructural and elemental changes induced by stabilization. Representative mixtures containing 9% silica fume (S-SF9, S-SF9-L9, and S-SF9-L9-PPF05) were analyzed after 7, 14 and 28 days of sealed curing. Representative fragments were collected from the internal region of the specimens, carefully fractured to expose fresh surfaces, mounted on holders, and gold-coated prior to imaging. SEM observations were performed at 500 and 1,500× magnification, and EDS was used to obtain qualitative elemental information from the analyzed areas.

4 Experiment results

4.1 Unconfined compressive strength and splitting tensile strength tests

The addition of silica fume (SF) alone resulted in a decrease in mechanical strength for both UCS and STS when compared to the soil (Tables 6 and 7, and Fig. 5). Without an

Table 6 Mean values (kPa) of the UCS (q_u), with corresponding 95% confidence intervals and coefficients of variation (COV)

Sample	0 days (kPa)	7 days (kPa)	14 days (kPa)	28 days (kPa)
Soil	1197 ± 101 (5.3%)	–	–	–
S-SF6	–	1113 ± 80 (4.52%)	1016 ± 83 (5.13%)	1071 ± 104 (6.10%)
S-SF9	–	907 ± 95 (6.58%)	911 ± 76 (5.25%)	910 ± 97 (6.7%)
S-SF12	–	832 ± 114 (8.59%)	831 ± 64 (4.84%)	819 ± 107 (8.22%)
S-SF6-L9	–	1658 ± 151 (5.73%)	1775 ± 74 (2.62%)	1804 ± 43 (1.5%)
S-SF9-L9	–	1652 ± 50 (1.90%)	1777 ± 66 (2.33%)	1894 ± 56 (1.86%)
S-SF12-L9	–	1571 ± 100 (4.00%)	1717 ± 73 (2.67%)	1875 ± 109 (3.66%)
S-SF6-L9-PPF05	–	1591 ± 75 (2.96%)	1678 ± 34 (1.27%)	1884 ± 62 (2.07%)
S-SF9-L9-PPF05	–	1584 ± 100 (3.97%)	1790 ± 30 (1.05%)	1875 ± 33 (1.11%)
S-SF12-L9-PPF05	–	1785 ± 57 (2.01%)	1906 ± 137 (4.52%)	1920 ± 41 (1.34%)

Table 7 Mean values (kPa) of the STS (q_t), with corresponding 95% confidence intervals and coefficients of variation (COV)

Sample	0 days (kPa)	7 days (kPa)	14 days (kPa)	28 days (kPa)
Soil	611 ± 49 (5.04%)	–	–	–
S-SF6	–	423 ± 21 (3.12%)	420 ± 36 (5.39%)	441 ± 32 (4.56%)
S-SF9	–	409 ± 45 (6.91%)	442 ± 31 (4.4%)	420 ± 19 (2.84%)
S-SF12	–	375 ± 43 (7.21%)	372 ± 35 (5.91%)	392 ± 12 (1.92%)
S-SF6-L9	–	891 ± 49 (3.46%)	1015 ± 72 (4.47%)	1051 ± 96 (5.74%)
S-SF9-L9	–	859 ± 113 (8.27%)	1029 ± 46 (2.81%)	1294 ± 112 (5.44%)
S-SF12-L9	–	799 ± 39 (3.07%)	1123 ± 66 (3.7%)	1325 ± 76 (3.61%)
S-SF6-L9-PPF05	–	817 ± 44 (3.42%)	893 ± 10 (0.7%)	989 ± 67 (4.26%)
S-SF9-L9-PPF05	–	813 ± 32 (2.48%)	852 ± 28 (2.07%)	982 ± 81 (5.18%)
S-SF12-L9-PPF05	–	848 ± 37 (2.75%)	875 ± 73 (5.24%)	1002 ± 91 (5.71%)

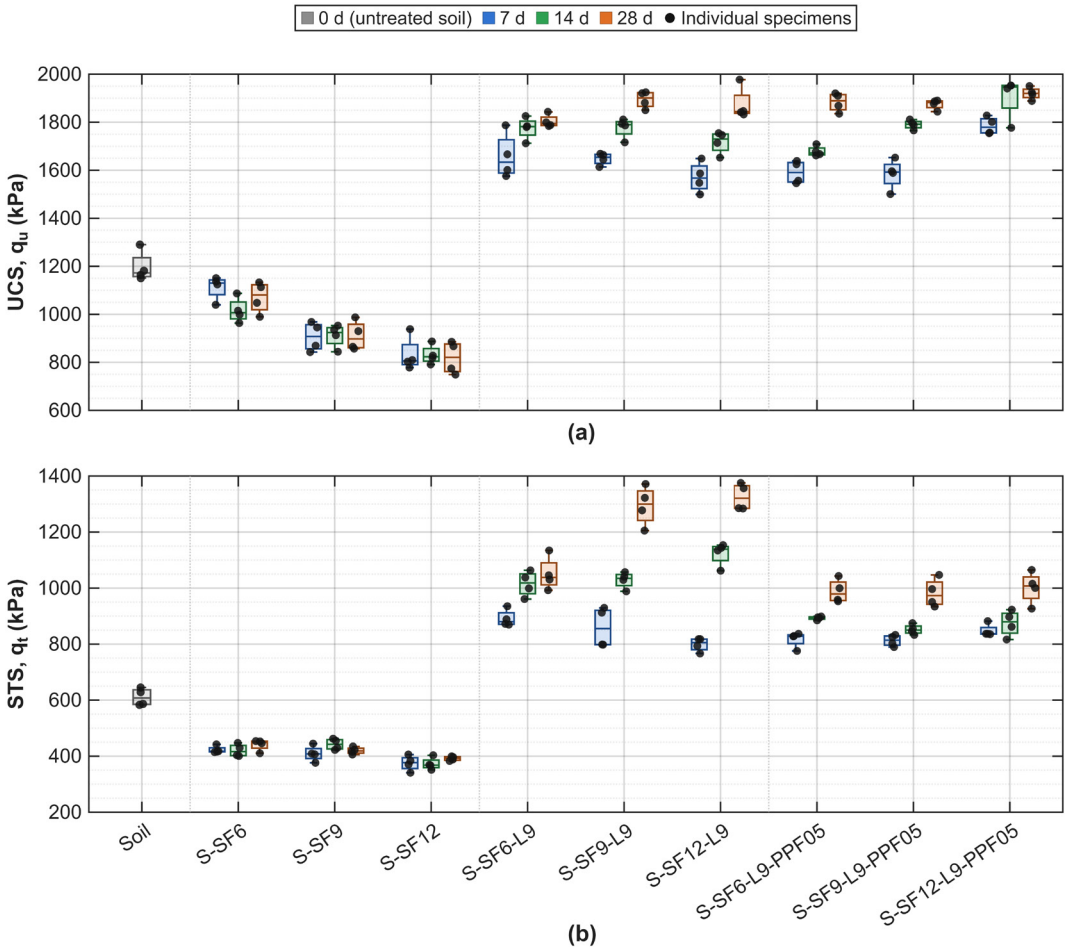

Fig. 5 Multifactorial box plots of the: (a) UCS results; (b) STS results

alkaline activator, the silica fume acts as an inert filler whose fine particles interfere with the inter-particle friction of the soil, thereby weakening its internal structure rather than providing a cementitious bond. As a pozzolanic material, silica fume requires a high-pH environment and a source of calcium to react and form strengthening compounds, conditions that are not met when it is added in isolation.

In contrast, the inclusion of lime was the factor for strength development. Lime acts as a chemical activator, providing the necessary alkalinity and calcium ions to initiate a pozzolanic reaction with the amorphous silica. This reaction forms a Calcium Silicate Hydrate (C–S–H) matrix that binds the soil particles, leading to a significant increase in both compressive and tensile strength over time. The highest STS was achieved in the S-SF12-L9 mixture (12% SF, 9% lime) with a value of (1325 ± 76) kPa, while the highest UCS was observed in the S-SF12-L9-PPF05 mixture (12% SF, 9% lime, 0.5% PPF) at (1920 ± 41) kPa.

Regarding the effect of polypropylene fibers (PPF) on the splitting tensile strength (q_t), the results presented in Table 7 indicate that the inclusion of 0.5% PPF does not lead to a uniform or statistically substantial reduction in peak strength across the evaluated mixtures. For instance, while the S-SF12-L9-PPF05 mixture at 28 days shows a numerical value of 1002 ± 91 kPa compared to the 1325 ± 76 kPa of the unreinforced S-SF12-L9 mixture, in most other configurations and curing ages, the variations remain within the experimental dispersion margins. This suggests that the fibers do not significantly alter the ultimate tensile capacity of the stabilized soil. The primary contribution of the PPF is observed in the post-peak regime (Fig. 6 (a) and (b)); while unreinforced specimens exhibit brittle failure with an immediate loss of load-bearing capacity, the fiber-reinforced specimens maintain structural integrity through a crack-bridging mechanism (Fig. 6 (b)). This transitions the failure mode towards a ductile behavior, which is a more significant mechanical enhancement than the marginal variations observed in the peak q_t values.

This change in failure mode is visually confirmed in Fig. 7. The unreinforced specimens failed catastrophically (Fig. 7 (a)), shattering under compression (bottom) and splitting completely in two under tension (top). In contrast, the fiber-reinforced specimens seemed unbroken after failure. Although cracked, they are held together by the fibers, which bridge the cracks and prevent complete separation. This enhancement of ductility is a known benefit of using PPF in Guabirotuba soil, preventing the abrupt failures typical of chemically stabilized soils [32, 33].

It is acknowledged that the UCS and STS tests were performed on unsaturated specimens, where matric suction contributes to the apparent strength. However, all specimens were molded and tested at comparable moisture contents and densities relative to their specific compaction curves. Therefore, the observed trends and the relative

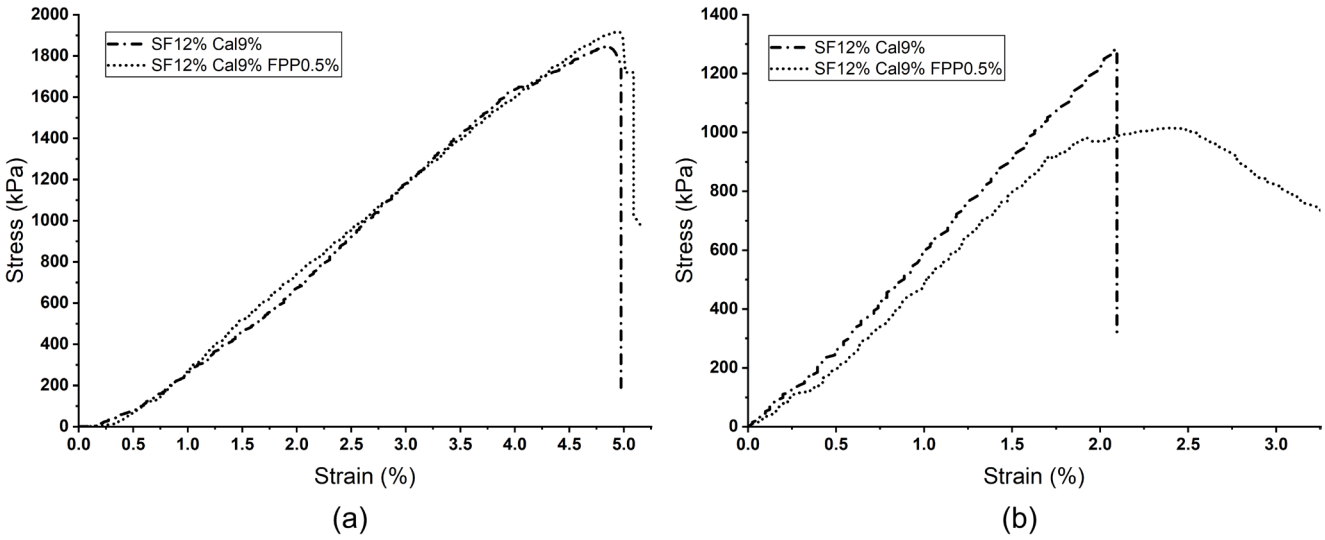

Fig. 6 Typical stress-strain curves of: (a) Unreinforced and fiber-reinforced in UCS test; (b) Unreinforced and fiber-reinforced in STS test

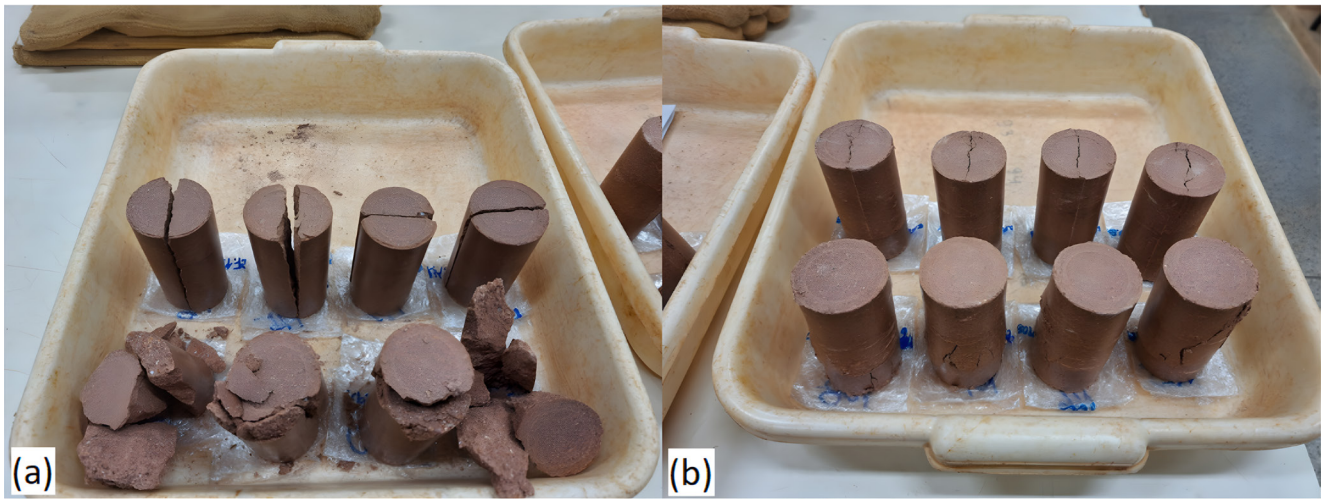

Fig. 7 Failure modes of specimens from STS (top) and UCS (bottom) tests: (a) Unreinforced; (b) Fiber-reinforced

improvement ratios provided by the stabilizers remain valid indicators of performance. Furthermore, the strength gains were subsequently validated under saturated conditions in the Consolidated Undrained (CU) triaxial tests, confirming that the improvements are due to hydraulic cementation and fiber reinforcement rather than suction alone. The UCS and saturated CU triaxial datasets do not permit a rigorous quantitative determination of matric suction.

The mechanical improvements achieved with the lime-SF-PPF ternary system are consistent with other studies. While other approaches evaluate 10% pumice powder for the long-term enhancement of contaminated clays [34], or the stabilization of oil-contaminated soils [35], the method proposed in this study demonstrates a significant acceleration in strength gain. Specifically, the lime-SF specimens achieved approximately 90% of their 28-day unconfined compressive strength within the first 7 days of curing.

This contrasts with stabilization using pumice powder, which is characterized by a slower pozzolanic reaction and requires extended curing periods, up to one year, to reach full microstructural maturation [34]. Furthermore, the addition of polypropylene fibers addresses the brittle failure, ensuring a ductile response that is not often found in stabilization alternatives.

4.2 Triaxial tests

The results of the consolidated undrained (CU) triaxial tests for the soil and the stabilized mixtures are presented in Figs. 8 to 11. Tests were conducted under confining pressures (σ_3) of 50, 100, 200 and 400 kPa. A summary of the effective shear strength parameters, cohesion (c') and friction angle (ϕ'), is provided in Table 8.

The inclusion of polypropylene fibers (PPF) resulted in an increase in effective cohesion (c') and a reduction in the effective friction angle (ϕ') compared to unreinforced specimens. The increase in c' is attributed to the mobilization of tensile strength in the fibers through crack-bridging, which provides an internal confinement that restricts lateral expansion. Micromechanically, the decrease in ϕ' occurs because the polymeric surface of the fibers presents a lower frictional resistance than the cemented soil grains, interfering with inter-particle interlocking along the shear plane. This reduction is substantiated by the dilation behavior observed in the CU tests. Under undrained

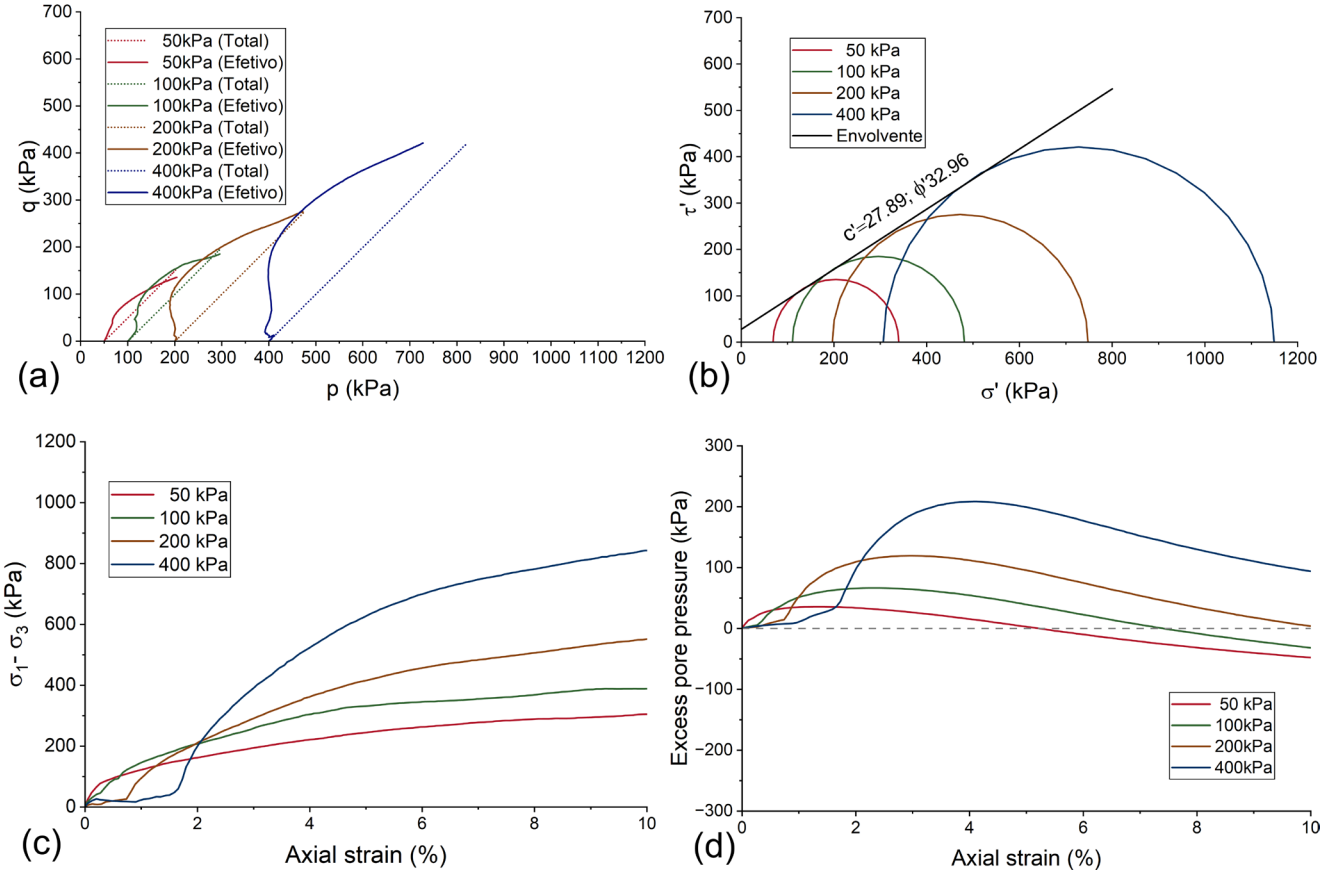

Fig. 8 Results of the Consolidated Undrained (CU) triaxial test for a soil sample compacted using modified effort: (a) Total and effective stresses path in the *p*-*q* plane; (b) Mohr–Coulomb effective stress circles and failure envelope; (c) Deviator stress versus axial strain; (d) Excess pore pressure versus axial strain

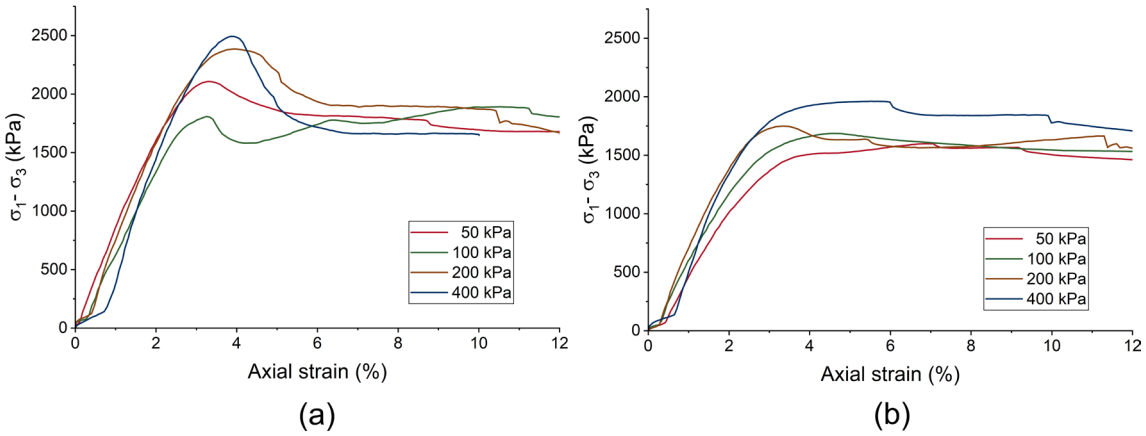

Fig. 9 Stress-strain behavior of mixtures: (a) S-SF6-L9; (b) S-SF6-L9-PPF05

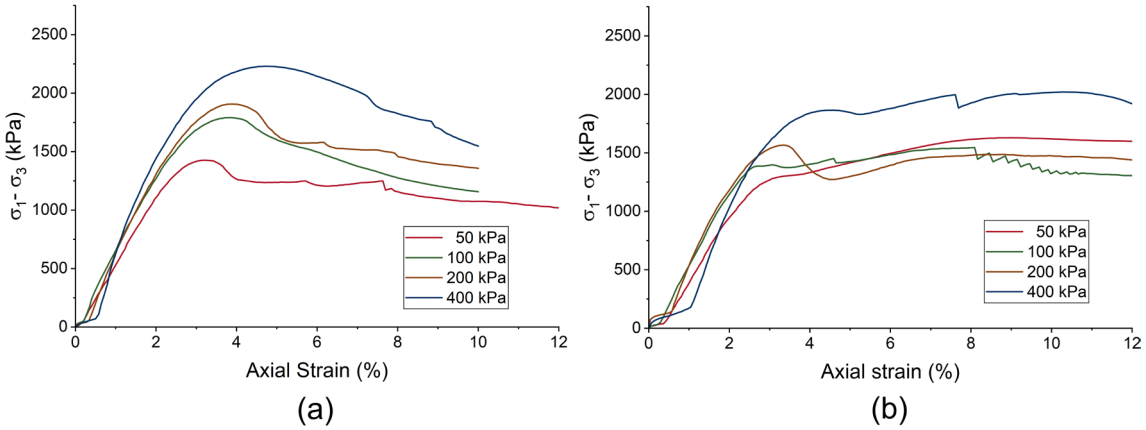

Fig. 10 Stress-strain behavior of mixtures: (a) S-SF9-L9; (b) S-SF9-L9-PPF05

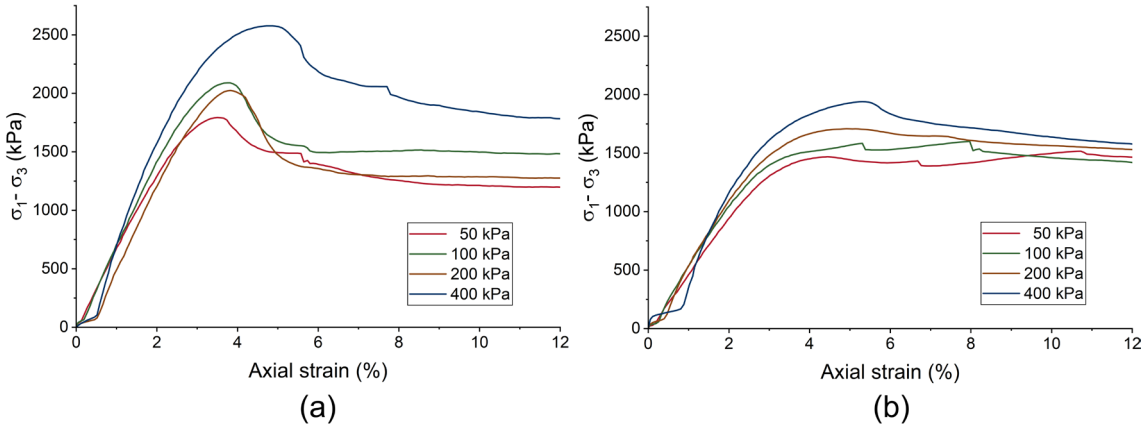

Fig. 11 Stress-strain behavior of mixtures: (a) S-SF12-L9; (b) S-SF12-L9-PPF05

Table 8 Triaxial CU test results for soil and blends

Sample	c' (kPa)	ϕ' (°)
Soil	27.89	32.96
S-SF6-L9	196.32	43.76
S-SF9-L9	212.62	37.73
S-SF12-L9	318.77	37.33
S-SF6-L9-PPF05	325.50	30.54
S-SF9-L9-PPF05	332.22	27.47
S-SF12-L9-PPF05	283.16	31.65

conditions, dilative tendency is evaluated through excess pore water pressure (Δu). As shown in the pore pressure responses (Figs. 12 to 14), fiber-reinforced specimens generated less negative excess pore pressure compared to unreinforced mixtures. This attenuated negative pore pressure indicates a lower tendency of the reinforced matrix to dilate during shear. A reduced dilation tendency inherently correlates with a lower effective friction angle.

The triaxial results suggest a change in dilative tendency among the mixtures. The unreinforced stabilized blends

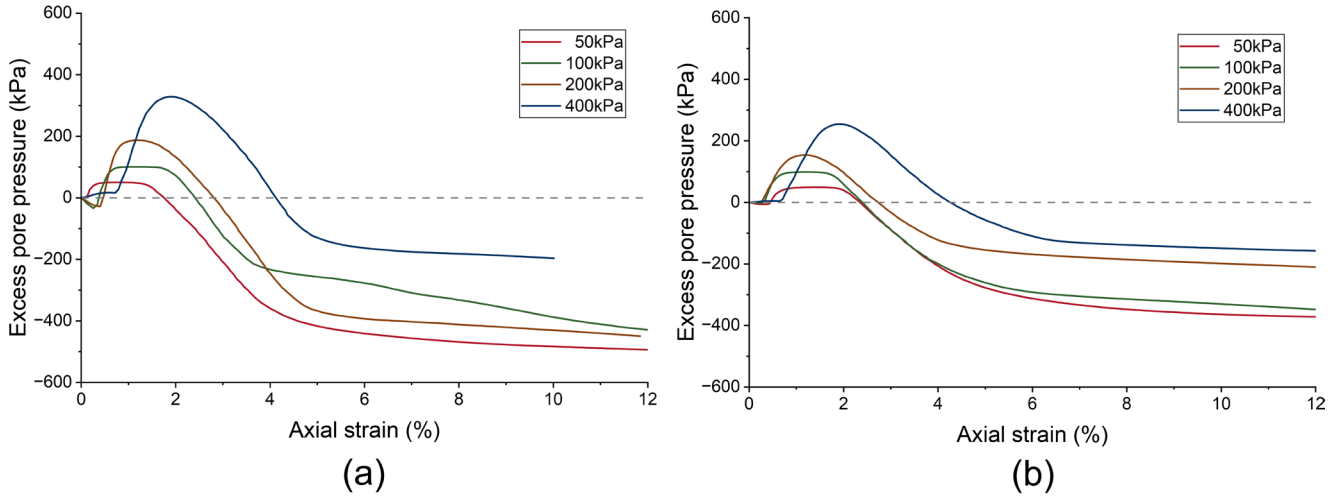

Fig. 12 Pore pressure response *vs*. axial strain for mixtures: (a) S-SF6-L9; (b) S-SF6-L9-PPF05

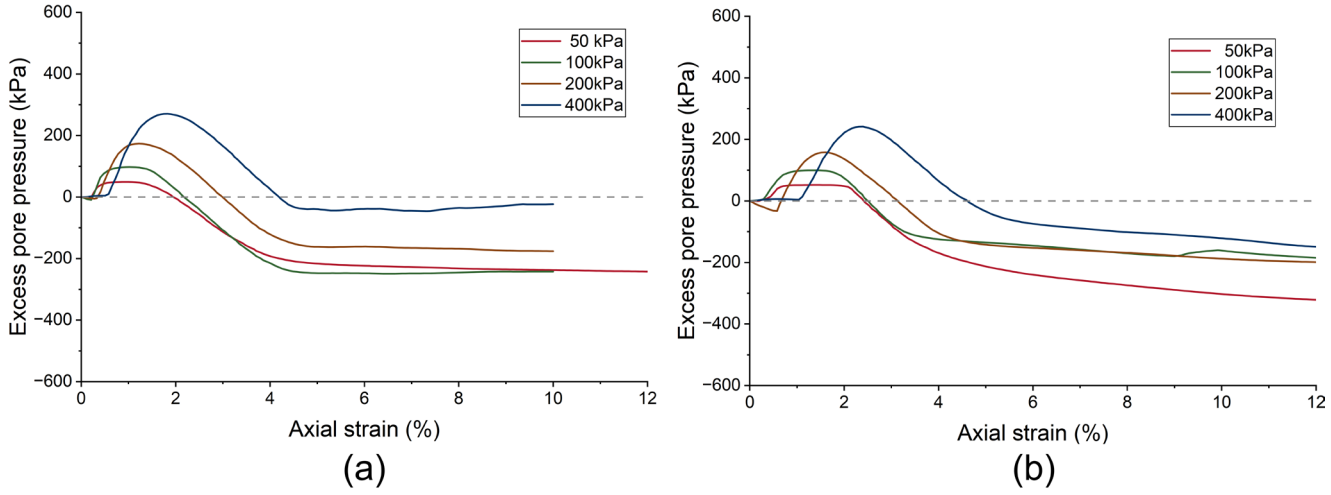

Fig. 13 Pore pressure response *vs*. axial strain for mixtures: (a) S-SF9-L9; (b) S-SF9-L9-PPF05

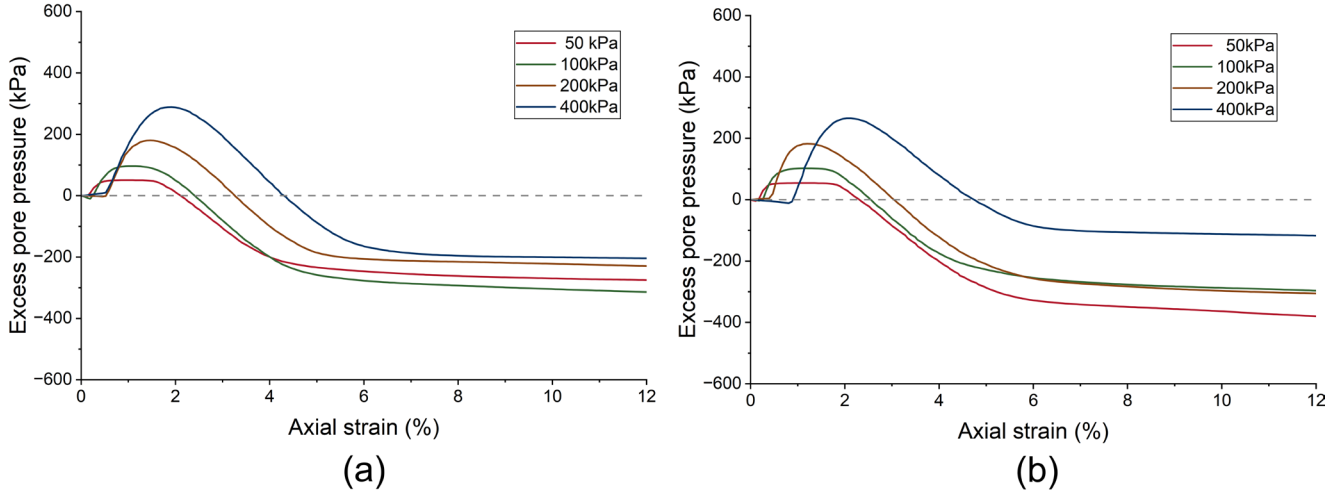

Fig. 14 Pore pressure response *vs*. axial strain for mixtures: (a) S-SF12-L9; (b) S-SF12-L9-PPF05

(e.g., $\phi' = 43.76°$ for S-SF6-L9), which exhibited steeper effective strength envelopes, also generated more pronounced negative excess pore pressures during CU shearing, indicating a stronger dilative tendency of the cemented matrix. In contrast, the fiber-reinforced mixtures showed lower peak effective friction angles (ranging from 27.47° to 31.65°) and reduced negative pore pressure generation, suggesting that the fibers modified the shear mechanism by reducing the relative contribution of dilation and increasing the apparent cohesive component. This interpretation

is qualitative, as no independent critical-state friction angle or explicit dilation angle was determined.

Regarding parameter fitting, it is important to note that for the more ductile responses observed in fiber-reinforced mixtures, the peak deviator stress was defined at the point of maximum resistance even if the failure was not abrupt. In cases where a clear peak was not reached, the stress at 15% axial strain was selected as the failure criterion. This criterion ensures consistency in the Mohr–Coulomb fit while acknowledging the sensitivity of the derived parameters to the selected stress range and the increased ductility.

Furthermore, while the increase in c' reflects the physical tensile reinforcement of the fibers acting on the cemented matrix [36], its magnitude is partially an artifact of the linear Mohr–Coulomb envelope fitting over the limited confining stress range evaluated (50 to 400 kPa). Since the true failure envelope of fiber-reinforced cemented soils typically exhibits non-linearity at very low confining stresses, linear extrapolation from this stress range may overestimate the true effective cohesion intercept.

The soil exhibited predominantly ductile, strain-hardening behavior, as shown in the test results summarized in Fig. 8. It did not show a well-defined peak strength; instead, it mobilized increasing resistance at axial strains greater than 8%. Throughout the shearing phase, the soil consistently generated positive excess pore pressure, indicating a contractive tendency under load. Its effective strength envelope was defined by $c' = 27.89$ kPa and $\phi' = 32.96°$.

Saran and Demiröz [37] investigated geopolymer-stabilized soil using a combination of lime, fly ash, silica fume, and basalt fibers. The authors carried out UCS and desiccation cracking tests at different additive contents. Saran and Demiröz [37] observed that fiber inclusion improves strength up to an optimal content, beyond which performance may decrease due to fiber clustering.

Syed et al. [38] also evaluated stabilized soil reinforced with treated fibers, combining experimental testing with machine learning-based prediction of strength parameters such as UCS, CBR, and consolidation. The authors utilized a local low plasticity clay, coal ash, silica fume, and banana fibers treated with alkaline solutions. The results confirmed that fiber reinforcement played a dominant role, improving ductility and post-peak behavior.

In contrast, all lime and silica fume-stabilized mixtures (S-SF6-L9 to S-SF12-L9) displayed a stiffer response, failing at much lower axial strains, typically between 2% and 5%. A key distinction from the soil was their dilatant behavior, characterized by the generation of negative excess pore pressure during shear, which increases the effective stresses. This evidence indicates that the cementitious matrix formed by the stabilizers must expand volumetrically to fail.

The primary influence of the polypropylene fibers (PPF) was on the post-peak behavior and the shear strength parameters. A comparative analysis of the stress-strain curves (Figs. 9 to 11) shows that while the unreinforced mixtures (S-SF6-L9, S-SF9-L9, S-SF12-L9) exhibited a brittle failure with a sharp drop in strength after the peak, the corresponding fiber-reinforced mixtures (S-SF6-L9-PPF05, S-SF9-L9-PPF05, and S-SF12-L9-PPF05) displayed a more ductile response, maintaining a significant residual strength.

This change in behavior is also reflected in the pore pressure response (Figs. 12 to 14). The fiber-reinforced samples generally showed a more attenuated generation of negative pore pressure, suggesting that the fibers help to control the volumetric expansion during shear.

To understand the failure mechanisms and the transition from contractive to dilative behavior, the total and effective stress paths in the p-q plane were analyzed. Figs. 15 to 17 present the stress paths for the mixtures containing 6%, 9% and 12% silica fume, respectively, comparing the unreinforced and fiber-reinforced conditions. During the initial stages of shearing, the effective stress paths (solid lines) for all stabilized mixtures migrate to the left. This indicates a contractive tendency accompanied by the generation of positive excess pore water pressure. As shearing progresses, the stress paths reach a distinct inflection point, known as the Phase Transformation State (PTS). At this point, the contractive behavior ceases, and the material begins to dilate, causing the stress paths to reverse direction and migrate to the right due to the generation of negative pore water pressure. When comparing the unreinforced and fiber-reinforced mixtures, the analysis reveals that the addition of polypropylene fibers (PPF) does not significantly alter the initial location of the PTS. This indicates that the onset of dilation is primarily governed by the stiffness of the cemented matrix (lime and silica fume). However, the fibers noticeably modify the stress path trajectory after the PTS point.

For the unreinforced mixtures (e.g., S-SF9-L9), the effective stress path climbs steeply after the PTS to reach a sharp peak strength, corresponding to a high effective friction angle. In contrast, for the fiber-reinforced mixtures (e.g., S-SF9-L9-PPF05), the post-PTS trajectory is attenuated. The fibers actively restrain the volumetric expansion through a tensile crack-bridging mechanism. This internal restriction alters the stress path slope near failure, allowing the material to mobilize a higher apparent cohesion (c') while flattening the overall failure envelope, which explains the reduction in the effective friction angle (ϕ'). Ultimately,

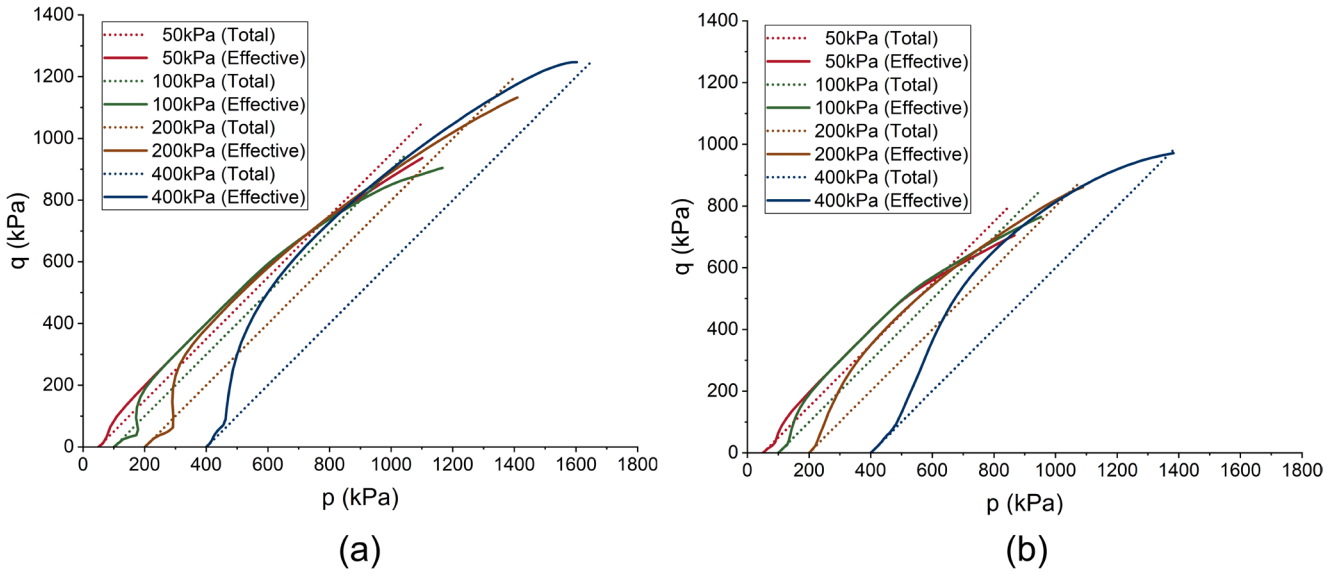

Fig. 15 Total and effective stress paths in: (a) *p-q* plane for unreinforced mixture S-SF6-L9; (b) Fiber-reinforced mixture S-SF6-L9-PPF05

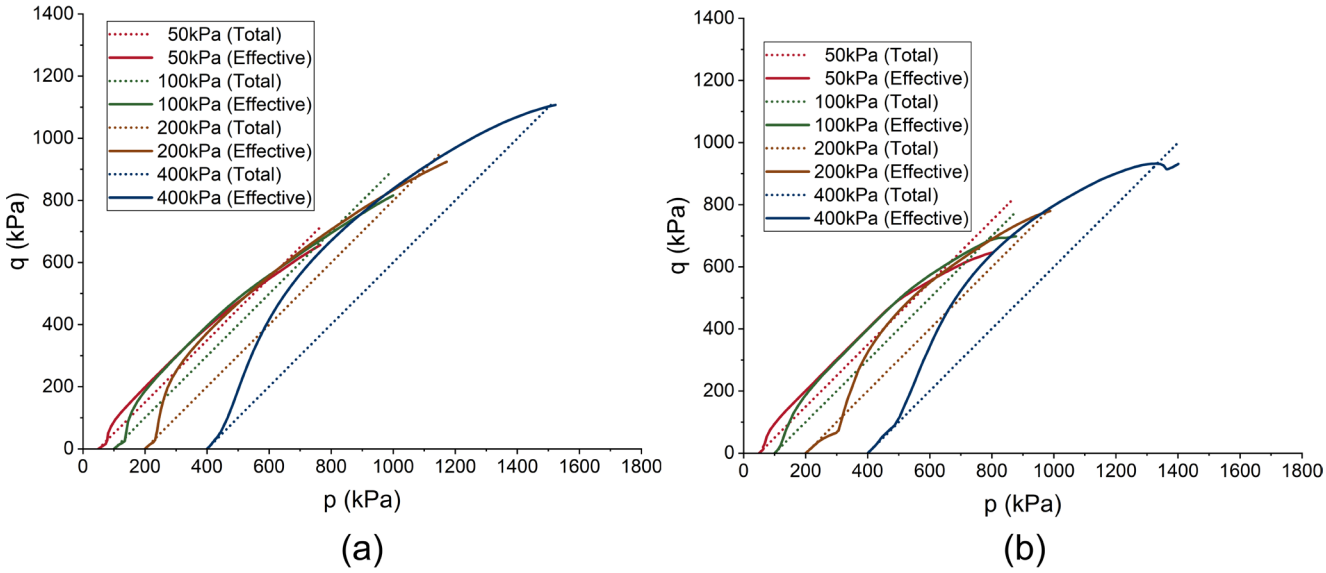

Fig. 16 Total and effective stress paths in: (a) *p-q* plane for unreinforced mixture S-SF9-L9; (b) Fiber-reinforced mixture S-SF9-L9-PPF05

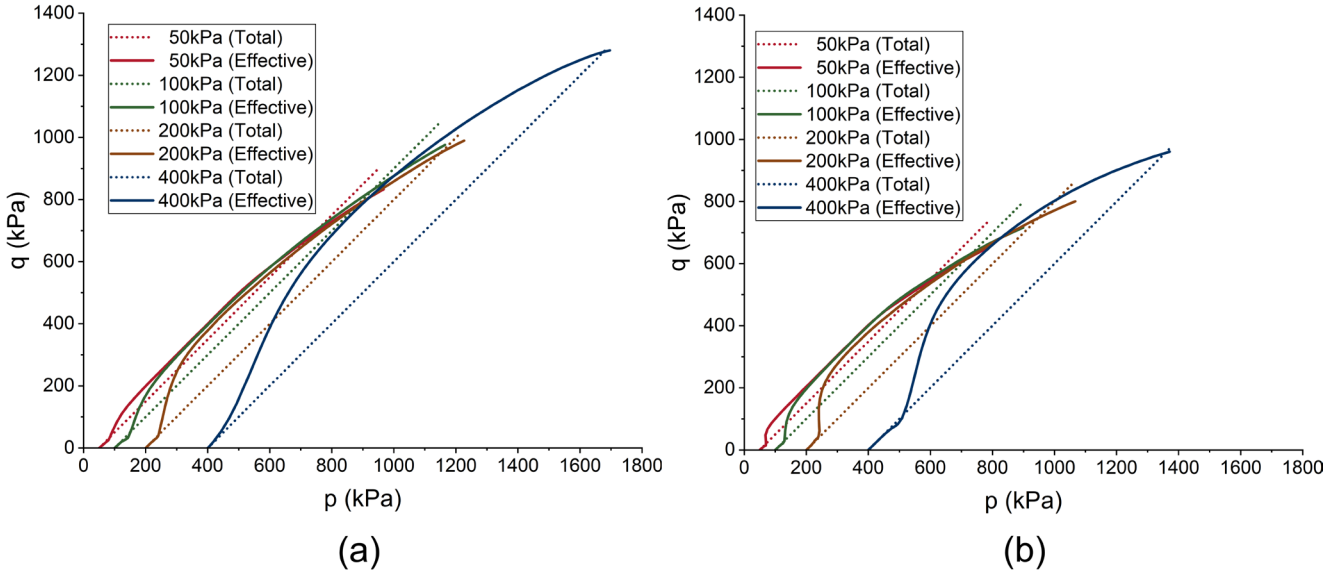

Fig. 17 Total and effective stress paths in: (a) *p-q* plane for unreinforced mixture S-SF12-L9; (b) Fiber-reinforced mixture S-SF12-L9-PPF05

all stabilized mixtures fail in a dilative state, but the PPF inclusion stabilizes this terminal dilative phase, providing the observed ductility. The peak failure states extracted from these stress paths are summarized by the effective failure envelopes in the p'-q plane (Fig. 18).

Analysis of the Mohr–Coulomb failure envelopes (Figs. 19 and 20) and the data in Table 8 reveals a trend regarding the strength parameters. The addition of fibers consistently led to an increase in effective cohesion (c') but a decrease in the effective friction angle (ϕ'). For instance, comparing mixture S-SF9-L9 (c' = 212.62 kPa, ϕ' = 37.73°) with S-SF9-L9-PPF05 (c' = 332.22 kPa, ϕ' = 27.47°), the cohesion increased while the friction angle was reduced.

This result suggests that the fibers contribute a tensile reinforcement mechanism that manifests as an apparent cohesion, but their presence may interfere with the particle-to-particle contact that governs frictional resistance. The overall strength envelopes, presented in the τ-σ' space in Figs. 19 and 20, summarize how the unreinforced mixtures tend to have a higher dependency on confining pressure (steeper slope), whereas the fiber-reinforced mixtures show a higher cohesion intercept.

While the standard CU triaxial tests provided the fundamental shear strength parameters for the stabilized mixtures, it is relevant to contextualize these results within the limitations of the testing apparatus. Standard triaxial tests impose fixed principal stress directions and boundary restraints at the end platens, which can influence the localized failure mechanisms. Literature evaluating torsional shear testing, such as the study by Khayat [39] on sandy soils under comparable confining stresses (100 to 400 kPa), demonstrates that the continuous rotation of principal stresses and inherent anisotropy influence the

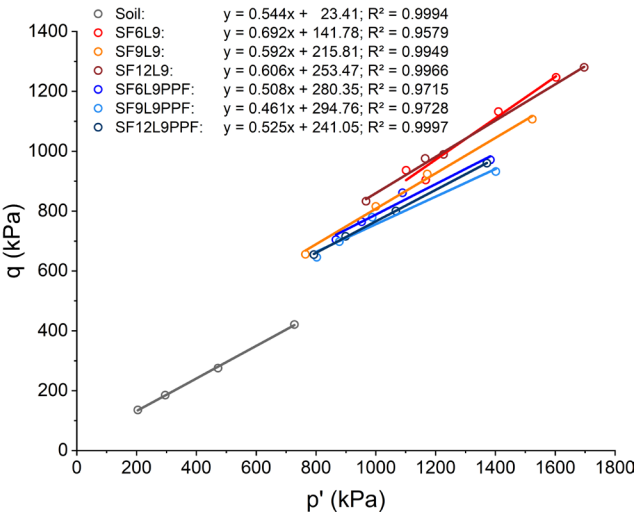

Fig. 18 Effective failure envelopes in the p'-q plane for the natural and stabilized soil

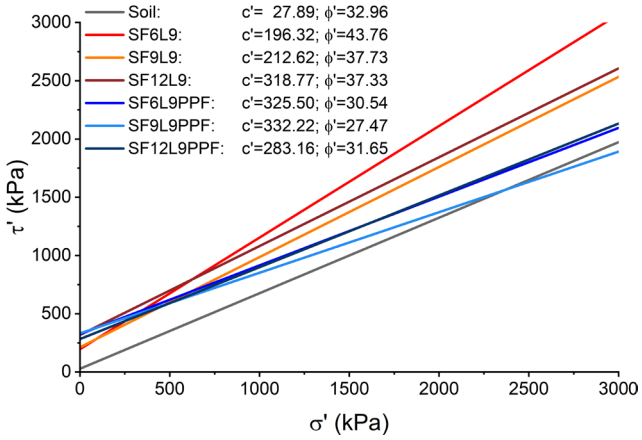

Fig. 19 Mohr–Coulomb failure envelopes for the materials

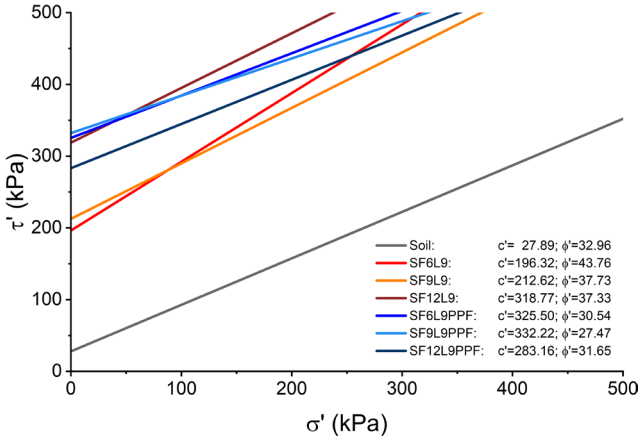

Fig. 20 Mohr–Coulomb failure envelopes with enlarged y-axis

volumetric behavior and shear response of granular materials. Although the cemented matrix of the lime-SF stabilized Guabirotuba soil limits the localized boundary effects typically observed in uncemented sands, the potential anisotropic yielding under complex stress paths remains a variable. Therefore, the derived c' and ϕ' parameters represent the macroscopic envelope under fixed principal stresses, whereas torsional loading could offer further insights into the anisotropic response of the fiber-reinforced composite.

Finally, it is important to acknowledge a limitation regarding the specimen preparation method and its influence on the mechanical response. The specimens were statically compacted in horizontal layers, a process known to induce a preferential horizontal orientation of the randomly distributed polypropylene fibers. Consequently, the stabilized composite inherently exhibits an anisotropic structure. Under standard triaxial loading, where the major principal stress (σ_1) is applied vertically, the shear failure plane develops at an angle relative to the horizontal plane. While the horizontally aligned fibers successfully intersect these shear planes, as evidenced by the transition

to ductile behavior and the significant increase in apparent cohesion (c'), the derived strength parameters represent this specific anisotropic condition. The structural performance of the material under different principal stress directions may vary due to this fiber alignment.

4.3 Microstructural analysis (SEM/EDS)

The microstructure of the mixture containing only soil and 9% SF is presented in Fig. 21. The micrograph reveals a porous and granular structure with no evidence of a cementing matrix, even after 28 days of curing. The corresponding EDS analysis, detailed in Table 9, confirms a near-total absence of available calcium. This lack of an alkaline activator prevents the pozzolanic reaction, explaining why no significant cementitious products were formed and, consequently, why no strength gain was observed in the mechanical tests.

The addition of 9% lime fundamentally transformed the material, as shown in Fig. 22. The micrograph displays a visibly denser and more homogeneous matrix, which is consistent with the expected pozzolanic interaction between the lime and the SF. This densification suggests the development

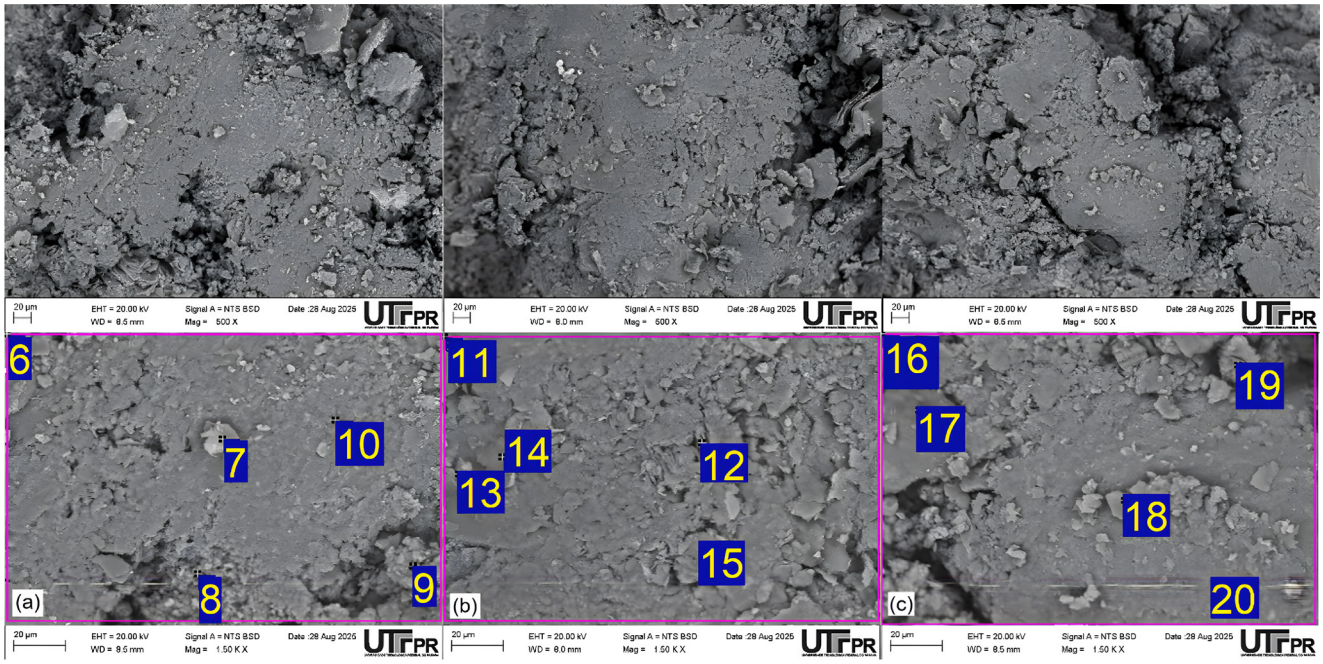

Fig. 21 SEM morphological analysis of the soil and 9% silica fume mixture at: (a) 7 days of curing (500×–1,500× magnification); (b) 14 days of curing (500×–1,500× magnification); (c) 28 days of curing (500×–1,500× magnification)

Table 9 Analysis by Energy-Dispersive X-ray Spectroscopy (EDS) of the soil and 9% silica fume mixture at at 7, 14, and 28 days of curing

Pos.	C	O	Al	Si	Fe
6	–	59.63	16.15	21.43	2.06
7	11.36	59.52	13.32	14.5	1.03
8	6.71	58.73	16.61	17.3	0.65
9	–	61.32	16.35	19.31	2.3
10	–	57.65	13.1	27.48	1.22
11	–	61.03	15.62	19.12	3.71
12	6.78	54.21	17.93	19.59	1.5
13	9.15	62.09	13.07	14.12	1.57
14	7.99	63.31	13.06	14.04	1.6
15	–	53.17	18.43	24.87	3.1
16	–	57.8	11.94	26.62	2.38
17	–	56.23	18.15	20.5	3.26
18	–	60.56	9.52	28.39	0.89
19	–	42.46	11.67	13.43	31.34
20	–	48.29	0.33	49.93	0.24

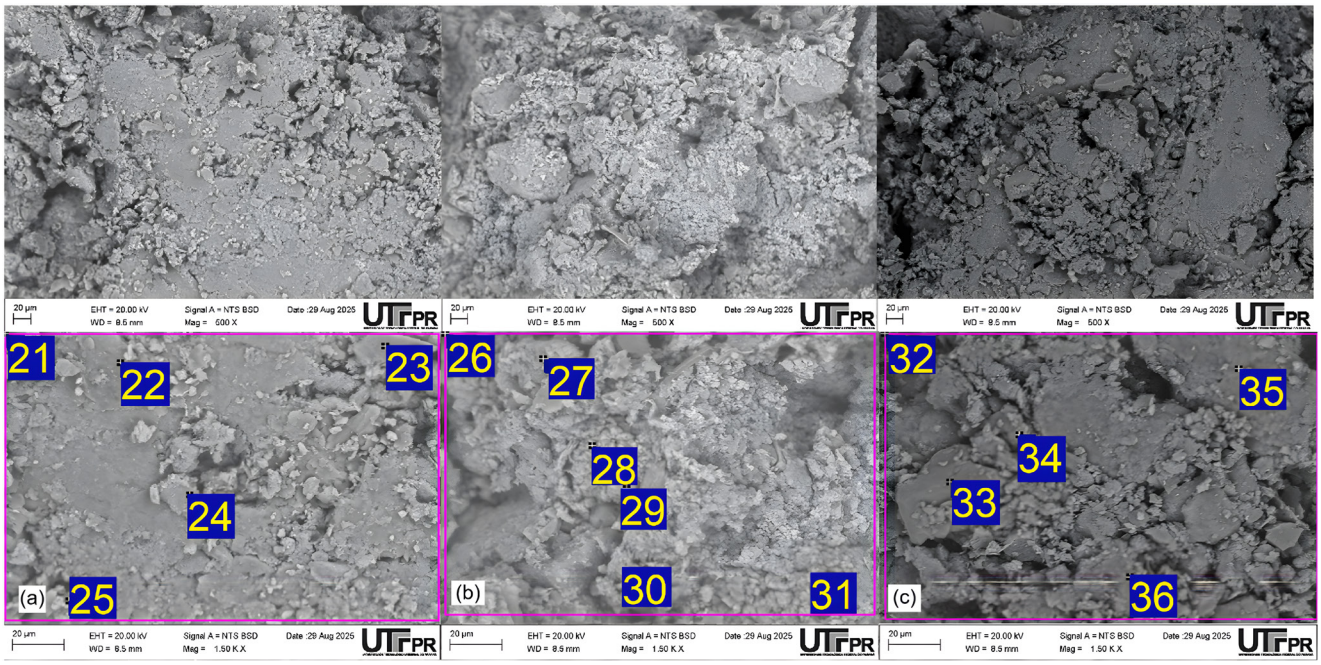

Fig. 22 SEM morphological analysis of the soil, 9% silica fume, and 9% lime mixture at: (a) 7 days of curing (500×–1,500× magnification); (b) 14 days of curing (500×–1,500× magnification); (c) 28 days of curing (500×–1,500× magnification)

of cementitious bonding products that fill voids and improve particle interconnection. The EDS results (Table 10) are an indirect evidence of microstructural densification associated with stabilization. Definitive phase characterization would require more specific analytical techniques, such as quantitative XRD or solid-state NMR.

This microstructural densification is the fundamental mechanism driving not only the enhanced unconfined compressive strength but also the expected long-term durability of the stabilized matrix. As the C–S–H gels bridge the pore spaces and encapsulate the soil particles, the composite becomes resistant to structural degradation over time. These observations align with recent durability-microstructure studies. For instance, Nasiri et al. [35] demonstrated that the progressive precipitation of cementitious gels in lime-stabilized soils governs their long-term performance and resistance to weathering over extended periods. Similarly, Li et al. [40] highlighted that the continuous formation of

Table 10 Analysis by Energy-Dispersive X-ray Spectroscopy (EDS) of the mixture of soil, 9% silica fume and 9% lime at 7, 14, and 28 days of curing

Pos.	C	O	Mg	Al	Si	Fe
21	–	61.43	1.57	13.31	16.89	2.38
22	25.27	44.33	9.6	3.55	4.35	0.77
23	7.69	58.74	0.18	15.48	16.85	0.92
24	11.58	47.67	0.75	13.41	17.33	2.55
25	–	63.85	1.6	2.71	24.96	0.63
26	–	62.57	2.83	13.09	15.03	2.89
27	17.81	59.36	9.71	1.85	2.28	0.48
28	–	62.85	2.34	12.94	14.36	4.16
29	8.83	54.05	0.32	16.48	18.42	1.57
30	–	59.28	1.77	15.96	17.98	2.61
31	–	64.16	–	15.82	18.47	1.12
32	–	60.41	1.42	13.1	20.53	2.56
33	10.66	57.31	–	0.53	31.35	0.16
34	–	63.85	0.8	15.37	17.2	2.22
35	10.7	39.55	–	20.09	25.97	3.12
36	10.52	42.52	0.58	18.46	22.12	4.77

C–S–H and C–A–S–H products significantly bolsters the durability and structural integrity of stabilized clays even under varying environmental and temperature conditions.

Finally, the interaction between the polypropylene fibers (PPF) and the stabilized matrix is illustrated in Fig. 23. The micrograph shows a fiber filament well-embedded within the dense matrix formed by the soil, lime, and SF. There is evidence of good adhesion at the fiber-matrix interface, which is crucial for the effectiveness of the reinforcement. This strong bond allows for the transfer of stresses across micro-cracks, which explains the transition from brittle to ductile behavior observed in the mechanical tests. As noted by Tang et al. [36], the strength of this soil-fiber interface is a controlling factor; in cemented soils, the accumulation of hydration products like CSH on the fiber surface creates a stronger bond than that found in unstabilized soil. The EDS data for this blend is provided in Table 11.

5 Conclusions

Based on the results obtained from the UCS, STS, CU triaxial, and SEM/EDS analyses, the following conclusions can be drawn regarding the stabilization of the Guabirotuba soil with lime, silica fume, and polypropylene fibers:

- The addition of silica fume (SF) alone was detrimental to the soil's mechanical properties, causing a consistent decrease in both Unconfined Compressive Strength (UCS) and Splitting Tensile Strength (STS). The inclusion of lime was a critical factor for stabilization; it acted as a chemical activator, enabling the pozzolanic reaction to form a Calcium Silicate Hydrate (C–S–H) matrix that bound the soil particles and led to significant gains in both compressive and tensile strength.
- The primary contribution of the polypropylene fibers (PPF) was not to the peak strength but to the material's ductility and post-peak behavior. The addition of fibers had an insignificant effect on peak UCS and resulted in a decrease in peak STS. However, the fibers fundamentally changed the failure mode from brittle to ductile in both test types. This conclusion was confirmed by the stress-strain curves, which showed a gradual reduction in post-peak resistance, and by the visual state of the specimens after failure, where fibers prevented catastrophic shattering and maintained structural integrity.
- In the consolidated undrained (CU) triaxial tests, all stabilized mixtures exhibited significantly higher shear strength properties than the soil. The addition of PPF consistently resulted in an increase in the effective cohesion (c') but a decrease in the effective friction angle (ϕ'). The highest effective cohesion of 332.22 kPa was recorded in the S-SF9-L9-PPF05

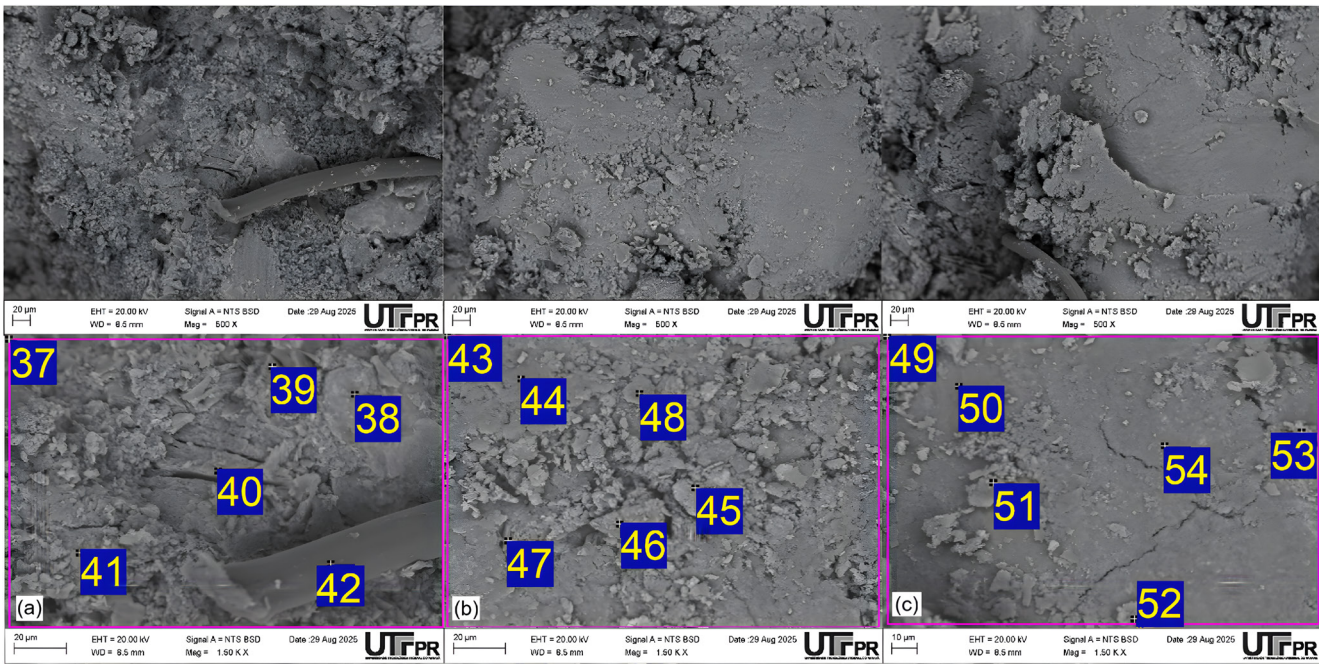

Fig. 23 SEM morphological analysis of the soil, 9% silica fume, 9% lime, and 0.5% polypropylene fibers mixture at: (a) 7 days of curing (500×–1,500× magnification); (b) 14 days of curing (500×–1,500× magnification); (c) 28 days of curing (500×–1,500× magnification)

Table 11 Energy Dispersive X-ray Spectroscopy (EDS) analysis of the mixture of soil, 9% silica fume, 9% lime and 0.5% polypropylene fibers at 7, 14, and 28 days of curing

Pos.	C	O	Al	Si	Ca	Fe
37	–	59.92	14.14	16.23	2.56	5.28
38	23.36	25.57	10.27	12.41	0.63	26.81
39	–	67.96	11.17	11.28	0.35	2.1
40	–	63.49	15.4	16.83	0.49	3.65
41	–	56.24	14.75	20.58	4.5	3.52
42	77.04	19.78	0.85	1.21	0.29	0.58
43	–	56.88	14.89	18.09	3.67	3.62
44	–	54.81	19.92	23.43	0.44	1.16
45	–	56.15	12.81	14.59	1.2	14.75
46	12.72	46.4	16.43	18.35	2.53	2.52
47	–	60.74	15.91	18.24	2.57	1.48
48	–	56.1	17.77	21.84	1.45	2.09
49	–	59.31	11.39	20.58	4.27	2.09
50	–	62.57	8.2	23.14	3.88	0.68
51	–	62.94	13.49	14.06	0.37	1.17
52	–	60.27	10.74	14.73	4.93	6.4
53	–	65.29	6.11	23.52	2.21	1.04
54	–	54.97	11.51	15.62	6.27	7.1

blend, a substantial increase from the soil's 27.89 kPa. This suggests the fibers contribute to a reinforcement mechanism that manifests as apparent cohesion but may interfere with the interparticle friction.

- The microstructural analyses (SEM/EDS) provided visual confirmation of the mechanical behavior. The micrographs showed that mixtures with only SF retained a porous, unreacted granular structure. In contrast, the addition of lime produced a dense, homogeneous CSH matrix. In the reinforced blends, the fibers were observed to be well-embedded within this dense matrix, demonstrating good adherence at the fiber-matrix interface, which is the mechanism responsible for the observed ductility.

Acknowledgement

The authors are thankful to the Federal University of Technology Paraná and the financial support that Coordination provided for the Improvement of Higher Education Personnel (CAPES). The authors acknowledge the use of an AI-based tool for spelling checks during the preparation of this manuscript.

References

[1] Xu, L., Wang, X., Qi, Y., Yuan, C., Ding, Z., Xu, R. "Strength Model for Cement-Stabilized Marine Clay: SEM Image Analysis and Microstructural Insights", Journal of Marine Science and Engineering, 13(2), 388, 2025. https://doi.org/10.3390/jmse13020388

[2] Wan, X., Ding, J., Jiao, N., Gao, M., Zhang, S. "Synergetic Effects of Alkaline and Sulfate-Based Waste Binders on Undrained Triaxial Behavior of Cement-Admixed Soft Clay", Journal of Materials in Civil Engineering, 36(11), 04024359, 2024. https://doi.org/10.1061/jmcee7.mteng-18057

[3] Lu, Z., Zhao, Y., Xian, S., Yao, H. "Experimental Study on Dynamic Resilient Modulus of Lime-Treated Expansive Soil", Advances in Materials Science and Engineering, 2020(1), 3272681, 2020. https://doi.org/10.1155/2020/3272681

[4] Corrêa-Silva, M., Araújo, N., Cristelo, N., Miranda, T., Gomes, A. T., Coelho, J. "Improvement of a clayey soil with alkali activated low-calcium fly ash for transport infrastructures applications", Road Materials and Pavement Design, 20(8), pp. 1912–1926, 2019. https://doi.org/10.1080/14680629.2018.1473286

[5] Zimar, Z., Robert, D., Zhou, A., Giustozzi, F., Setunge, S., Kodikara, J. "Application of coal fly ash in pavement subgrade stabilisation: A review", Journal of Environmental Management, 312, 114926, 2022. https://doi.org/10.1016/j.jenvman.2022.114926

[6] Baldovino, J. d. J. A., Izzo, R. L. d. S., Rose, J. L. "Advances on dosages for cement stabilized rammed guabirotuba silt depending on climate conditions", Soils and Rocks, 43(4), pp. 631–645, 2020. https://doi.org/10.28927/SR.434631

[7] Arrieta Baldovino, J. d. J., dos Santos Izzo, R. L., da Silva, É. R., Lundgren Rose, J. "Sustainable Use of Recycled-Glass Powder in Soil Stabilization", Journal of Materials in Civil Engineering, 32(5), 04020080, 2020. https://doi.org/10.1061/(asce)mt.1943-5533.0003081

[8] Almuaythir, S., Zaini, M. S. I., Hasan, M., Hoque, M. I. "Sustainable soil stabilization using industrial waste ash: Enhancing expansive clay properties", Heliyon, 10(20), e39124, 2024. https://doi.org/10.1016/j.heliyon.2024.e39124

[9] Türköz, M., Umu, S. U., Öztürk, O. "Effect of Silica Fume as a Waste Material for Sustainable Environment on the Stabilization and Dynamic Behavior of Dispersive Soil", Sustainability, 13(8), 4321, 2021. https://doi.org/10.3390/su13084321

[10] Yuan, K., Ni, W., Zhao, L., Wang, H. "Silica fume stabilized loess: Mechanical properties, microstructural evolution and environmental analysis", Sustainable Materials and Technologies, 36, e00604, 2023. https://doi.org/10.1016/j.susmat.2023.e00604

[11] Ghavami, S., Naseri, H., Jahanbakhsh, H., Moghadas Nejad, F. "The impacts of nano-SiO_2 and silica fume on cement kiln dust treated soil as a sustainable cement-free stabilizer", Construction and Building Materials, 285, 122918, 2021. https://doi.org/10.1016/j.conbuildmat.2021.122918

[12] Hou, D., Ma, H., Li, Z., Jin, Z. "Molecular simulation of "hydrolytic weakening": A case study on silica", Acta Materialia, 80, pp. 264–277, 2014. https://doi.org/10.1016/j.actamat.2014.07.059

[13] Ferreira, F. A., Desir, J. M., Lima, G. E. S. d., Pedroti, L. G., Franco de Carvalho, J. M., Lotero, A., Consoli, N. C. "Evaluation of mechanical and microstructural properties of eggshell lime/rice husk ash alkali-activated cement", Construction and Building Materials, 364, 129931, 2023. https://doi.org/10.1016/j.conbuildmat.2022.129931

[14] Xiao, R., Polaczyk, P., Jiang, X., Zhang, M., Wang, Y., Huang, B. "Cementless controlled low-strength material (CLSM) based on waste glass powder and hydrated lime: Synthesis, characterization and thermodynamic simulation", Construction and Building Materials, 275, 122157, 2021. https://doi.org/10.1016/j.conbuildmat.2020.122157

[15] Navagire, O. P., Srinivasan, V., Patel, A., Gowrisankar, D. "Stabilization of Expansive Soils Using Polypropylene Fiber for Enhanced Engineering Properties: A Study on Black Cotton Soils from India", Indian Geotechnical Journal, 56(3), pp. 1445–1461, 2026. https://doi.org/10.1007/s40098-025-01225-3

[16] Dou, H., Xu, B., Li, F., Li, Y., Liu, H., Zu, F. "Research and application of fiber-reinforced EPS particle lightweight soil in highway engineering in cold regions", Scientific Reports, 15(1), 25264, 2025. https://doi.org/10.1038/s41598-025-10866-6

[17] Medina-Martinez, C. J., Sandoval-Herazo, L. C., Zamora-Castro, S. A., Vivar-Ocampo, R., Reyes-Gonzalez, D. "Natural Fibers: An Alternative for the Reinforcement of Expansive Soils", Sustainability, 14(15), 9275, 2022. https://doi.org/10.3390/su14159275

[18] Hejazi, S. M., Sheikhzadeh, M., Abtahi, S. M., Zadhoush, A. "A simple review of soil reinforcement by using natural and synthetic fibers", Construction and Building Materials, 30, pp. 100–116, 2012. https://doi.org/10.1016/j.conbuildmat.2011.11.045

[19] Mir Moayed, S. A., Arabani, M., Ahmadi, H. "Strength Parameters of Kaolinite Clay Stabilized with Nano-Silica and Reinforced with Hemp Fibers under Freeze-Thaw Cycles: An Experimental Study", International Journal of Engineering, Transactions C: Aspects, 39(3), pp. 639–657, 2026. https://doi.org/10.5829/ije.2026.39.03c.07

[20] Zaid, M., Rizvi, Z., Basu, D., Wuttke, F. "Optimizing the fracture resistance of clay liners through fiber content and moisture control", Scientific Reports, 15(1), 32443, 2025. https://doi.org/10.1038/s41598-025-17178-9

[21] Callesen, I., Palviainen, M., Armolaitis, K., Rasmussen, C., Kjønaas, O. J. "Soil texture analysis by laser diffraction and sedimentation and sieving–method and instrument comparison with a focus on Nordic and Baltic forest soils", Frontiers in Forests and Global Change, 6, 1144845, 2023. https://doi.org/10.3389/ffgc.2023.1144845

[22] Saminpanya, S., Denkitkul, N. "Micromorphology, mineralogy, and geo-chemistry of sediments at the Tham Lod rock shelter archaeological site in Mae Hong Son, Thailand: Suggestions of a late Pleistocene climate", Journal of Cave and Karst Studies, 82(1), pp. 51–68, 2020. https://doi.org/10.4311/2019ES0111

[23] Hasan, M., Zaini, M. S. I., Yie, L. S., Masri, K. A., Putra Jaya, R., Hyodo, M., Winter, M. J. "Effect of optimum utilization of silica fume and eggshell ash to the engineering properties of expansive soil", Journal of Materials Research and Technology, 14, pp. 1401–1418, 2021. https://doi.org/10.1016/j.jmrt.2021.07.023

[24] Purba, D. A., Syahril, Sagala, S. D., Hamdhan, I. N. "The effectiveness of silica fume and calcite in improving the shear strength of clay soil", Brazilian Journal of Development, 11(5), e79469, 2025. https://doi.org/10.34117/bjdv11n5-007

[25] Baldovino, J. J. A., Izzo, R. L. S., Rose, J. L., Domingos, M. D. I. "Strength, durability, and microstructure of geopolymers based on recycled-glass powder waste and dolomitic lime for soil stabilization", Construction and Building Materials, 271, 121874, 2021. https://doi.org/10.1016/j.conbuildmat.2020.121874

[26] Baldovino, J. A., Moreira, E. B., Teixeira, W., Izzo, R. L. S., Rose, J. L. "Effects of lime addition on geotechnical properties of sedimentary soil in Curitiba, Brazil", Journal of Rock Mechanics and Geotechnical Engineering, 10(1), pp. 188–194, 2018. https://doi.org/10.1016/j.jrmge.2017.10.001

[27] Ranjbar, N., Mehrali, M., Behnia, A., Javadi Pordsari, A., Mehrali, M., Alengaram, U. J., Jumaat, M. Z. "A Comprehensive Study of the Polypropylene Fiber Reinforced Fly Ash Based Geopolymer", PLoS One, 11(1), e0147546, 2016. https://doi.org/10.1371/journal.pone.0147546

[28] Diniz, B. C., Fedrigo, W., Kleinert, T. R., Batista, G. d. S., Núñez, W. P., Correa, B. M., Brito, L.A.T. "Lime Stabilization of Tropical Soil for Resilient Pavements: Mechanical, Microscopic, and Mineralogical Characteristics", Materials, 17(19), 4720, 2024. https://doi.org/10.3390/ma17194720

[29] ASTM International "ASTM D1557-12(2021) Standard Test Methods for Laboratory Compaction Characteristics of Soil Using Modified Effort (56,000 ft-lbf/ft^3 (2,700 kN-m/m^3))", ASTM International, West Conshohocken, PA, USA, 2021. https://doi.org/10.1520/D1557-12R21

[30] ISO "ISO 2602:1980 Statistical interpretation of test results — Estimation of the mean — Confidence interval", International Organization for Standardization, Geneva, Switzerland, 1980.

[31] ABNT "NBR 12025: Solo-cimento — Ensaio de compressão simples de corpos de prova cilíndricos — Método de ensaio" (NBR 12025: Soil-cement — Simple compression test of cylindrical specimens — Test method), Associação Brasileira de Normas Técnicas, Rio de Janeiro, Brazil, 2012. (in Portuguese)

[32] Muñoz, Y. O., de Almeida, J. L., Mora, A. J. E. V., Pudell, P. C. A., Baldovino, J. A., dos Santos Izzo, R. L. "The Behavior of Stabilized Reinforced Soil for Road Embankments Application", Geotechnical and Geological Engineering, 41(4), pp. 2599–2628, 2023. https://doi.org/10.1007/s10706-023-02416-6

[33] Almeida, J. L. d., Ordoñez, Y. M., Pudell, P. C. A., Brandão, D. L., Orioli, M. A., Izzo, R. L. d. S. "Improvements in the mechanical behavior of a silty soil treated with rice husk silica, lime, and polypropylene fiber", International Journal of Geotechnical Engineering, 17(3), pp. 283–297, 2023. https://doi.org/10.1080/19386362.2023.2227503

[34] Nasiri, H., Khayat, N., Nazarpour, A. "Assessing one-year effects of 10 % pumice powder on strength and microstructure of contaminated clay (Case Study: Ahvaz Project, Iran)", Case Studies in Construction Materials, 21, e03892, 2024. https://doi.org/10.1016/j.cscm.2024.e03892

[35] Nasiri, H., Khayat, N., Nazarpour, A. "Utilization of the oil-contaminated soil as a sustainable resource in rural road construction and rehabilitation in oil-producing countries", Journal of Cleaner Production, 483, 144175, 2024. https://doi.org/10.1016/j.jclepro.2024.144175

[36] Tang, C., Shi, B., Gao, W., Chen, F., Cai, Y. "Strength and mechanical behavior of short polypropylene fiber reinforced and cement stabilized clayey soil", Geotextiles and Geomembranes, 25(3), pp. 194–202, 2007. https://doi.org/10.1016/j.geotexmem.2006.11.002

[37] Saran, O., Demiröz, A. "Strength Improvement and Crack Mitigation in Clay Soil Using Basalt Fiber and Pozzolanic Additives", Geotechnical and Geological Engineering, 43(7), 367, 2025. https://doi.org/10.1007/s10706-025-03346-1

[38] Syed, M., Ashfaq, M., Jamhiri, B., Ali, U., Jalal, F. E. "Sustainable engineering of fiber-reinforced geopolymer-treated low plasticity clay linking geomechanics and microstructure through support vector machines", Scientific Reports, 15(1), 44399, 2025. https://doi.org/10.1038/s41598-025-28438-z

[39] Khayat, N. "Monotonic behaviour of sand under torsional loading with different confine stress", International Journal of GEOMATE, 14(43), pp. 148–153, 2018. https://doi.org/10.21660/2018.43.7359

[40] Li, Z., Wang, J., Chen, J., Liang, Y., Xie, S., Li, Q., Du, X., Jiang, Z., Zhu, Y., Ni, H. "Characteristics and mechanisms of sustainable recovery of perlite from carrageenan residue by green technology and its application in carrageenan extraction", Journal of Cleaner Production, 434, 140131, 2024. https://doi.org/10.1016/j.jclepro.2023.140131